Local buckling of stainless steel I-sections in fire: finite element modelling and design

Zhe Xing[a], Merih Kucukler[b,*], Leroy Gardner[a]

[a]*Department of Civil and Environmental Engineering, Imperial College London, London SW7 2AZ, UK*
[b]*School of Engineering, University of Warwick, Coventry, CV4 7AL, UK*

Abstract

The structural response of stainless steel I-sections in fire is investigated in this paper. Finite element models of stainless steel I-section members, capable of replicating their cross-section behaviour at elevated temperatures, are created and validated against existing experimental data from the literature. The validated finite element models are then utilised to perform comprehensive numerical parametric studies, where over 1000 numerical simulations of the response of stainless steel I-sections in fire are carried out, considering different cross-section dimensions, loading conditions, stainless steel grades and elevated temperature levels. On the basis of the findings from the parametric studies, the existing design rules of the European structural steel fire design standard EN 1993-1-2 and the recent design recommendations of [1], together with the plastic effective width method of [2], are assessed in terms of their accuracy and reliability. It is observed that relative to the existing fire design rules set out in EN 1993-1-2, the design methods of Xing et al. [1] and Bambach and Rasmussen [2] are able to provide more accurate and reliable ultimate cross-section resistance predictions for stainless steel I-sections in fire, providing further verification of the suitability of the design provisions of [1] for inclusion in the next revision of EN 1993-1-2.

Keywords: Cross-section behaviour; Eurocode; Fire; Finite element modelling; I-section; Local buckling; Plastic effective width method; Stainless steel

1. Introduction

Welded stainless steel I-section members are being increasingly used in structural applications owing to their durability and high load-bearing capacities relative to those achieved by the more conventionally adopted cold-formed tubular members [3–5]. Stainless steel I-section members are often prone to local instability effects that prevent the attainment of their full cross-section resistances; consideration should therefore be given to such effects in both room temperature and elevated temperature design. The European structural stainless steel design standard EN 1993-1-4 [6] provides effective width-based design rules, underpinned by extensive research [7–10], for

*Corresponding author
Email addresses: zhe.xing16@imperial.ac.uk (Zhe Xing), merih.kucukler@warwick.ac.uk (Merih Kucukler), leroy.gardner@imperial.ac.uk (Leroy Gardner)

the treatment of local buckling at room temperature. These rules are also adopted in the European structural steel fire design standard EN 1993-1-2 [11] for the local buckling assessment of stainless steel sections in fire. However, since the material response of stainless steel at elevated temperatures is significantly different from that at room temperature, these existing provisions [11] generally yield somewhat inaccurate and scattered resistance predictions for stainless steel cross-sections in fire, highlighting the need for specific local buckling rules for the design of stainless steel cross-sections at elevated temperatures.

Thus far, although some post-fire research studies have been conducted [12, 13], there have been relatively few studies into the cross-section behaviour of stainless steel I-section members in fire. Gardner and Baddoo [14] conducted a series of physical tests on stainless steel I-sections under major axis bending at elevated temperatures. Lopes et al. [15] performed a numerical investigation into the behaviour of stainless steel I-sections subjected to major axis bending in fire, observing that the ultimate cross-section resistances predicted through the provisions of EN 1993-1-2 [11] were generally inaccurate. Xing et al. [1] proposed a new effective width-based design approach for the local buckling assessment of stainless steel plates in fire, in which the variation in strength and stiffness of stainless steel at different elevated temperature levels is taken into account. However, the study of Xing et al. [1] largely considered individual plate elements; in the present paper, the elevated temperature local buckling behaviour and design of full structural stainless steel I-sections under compression and bending about both principal axes are examined.

A comprehensive numerical study focusing on the cross-section behaviour of stainless steel I-sections in fire is first carried out in this paper. Finite element models that are able to capture the cross-section response of stainless steel I-section members are created and validated against a series of experimental results from the literature. Parametric studies are then carried out to generate extensive fundamental structural performance data, covering a wide range of stainless steel grades, elevated temperature levels, cross-section geometries and loading conditions. Assessment of the design provisions in the current European structural steel fire design standard EN 1993-1-2 [11] and those proposed by Xing et al. [1] is subsequently carried out through comparisons against the obtained numerical data. For stainless steel I-sections subjected to minor axis bending in fire, the plastic effective width method of [2], originally developed to determine the room temperature minor axis bending moment resistances of carbon steel sections [16], is also evaluated and shown to provide accurate results. Finally, a reliability assessment is presented.

2. Finite element modelling

In this section, finite element models that are able to replicate the cross-section behaviour of stainless steel I-section members at elevated temperatures are developed and validated against a series of experimental results from the literature. The validated finite element models are used to assess the accuracy of the current design provisions given in EN 1993-1-2 [11], as well as the design proposals of Xing et al. [1] and Bambach and Rasmussen [2].

2.1. Development of finite element models

The numerical simulations were carried out using the finite element analysis software Abaqus [17]. The S4R element – a four-noded reduced integration general purpose shell finite element –

was adopted in the finite element modelling; this element has been successfully utilised in similar previous applications [18–22]. To accurately capture the cross-section behaviour of stainless steel I-sections in fire, twenty elements were employed across each web plate; the number of the elements across each flange plate and along the length of the members was selected such that the aspect ratios of the elements were equal to unity [23]. Note that the member length L to cross-section depth h ratios L/h were equal to 3.0 (i.e. $L/h = 3.0$) for all the created models; thus, sixty elements were used along the length of the members.

The boundary conditions adopted in the numerical models are illustrated in Fig. 1. As can be seen in Fig. 1 (a), to simulate the structural response of stainless steel I-sections subjected to compression, the displacements and rotations of the end cross-sections were linked to two concentric reference points (i.e. reference point 1 and reference point 2) through rigid body kinematic coupling constraints; all degrees of freedoms of the two reference points were restrained except for the longitudinal translation (U1) of the reference point 1. Compression was applied as a point force equal to $Af_{2,\theta}$ to reference point 1, where A is the gross cross-section area and $f_{2,\theta}$ is the elevated temperature material strength at 2% total strain. Similar boundary conditions as those for the models under compression were also adopted in the models of I-sections under bending but with two differences: (i) the rotations about axis 2 (UR2) at the two reference points for major axis bending (see Fig. 1 (b)) and the rotations about axis 3 (UR3) at the two reference points for minor axis bending (see Fig. 1 (c)) were released to ensure that the models were free to rotate about their respective axis of bending and (ii) the longitudinal translation (U1) of the node at the centre of the web at the mid-span section was restrained instead of the longitudinal translation (U1) of reference point 2. Bending moments equal to $W_{\mathrm{pl}}f_{2,\theta}$ were applied to reference points 1 and 2 in the models of I-sections under bending, where W_{pl} is the plastic section modulus.

Local geometric imperfections were taken into consideration in the finite element models as shown in Fig. 2, in accordance with EN 1993-1-5 [24], where local imperfections with sinusoidal half-wavelengths equal to the plate widths b were applied to the models. The local imperfection magnitude of the plate with lower elastic buckling stress was first determined in accordance with EN 1993-1-5 [24] – the flange imperfection $e_{0,\mathrm{f}}$ was scaled to 1/50 of the half flange width (i.e. $e_{0,\mathrm{f}} = b_{\mathrm{f}}/50$) when the elastic buckling stress of the flanges was lower than that of the web (i.e. $\sigma_{\mathrm{cr,f}} < \sigma_{\mathrm{cr,w}}$), while the web imperfection $e_{0,\mathrm{w}}$ was scaled to 1/200 of the web height (i.e. $e_{0,\mathrm{w}} = b_{\mathrm{w}}/200$) when the elastic buckling stress of the web was lower than that of the flanges (i.e. $\sigma_{\mathrm{cr,w}} < \sigma_{\mathrm{cr,f}}$); even though actual imperfection magnitudes vary in practice, these values provide conservative estimations of their magnitudes [24]. The local imperfection magnitude of the plate with the higher elastic buckling stress was determined such that the angle of the web-flange junction remained at 90°.

The stress-strain (σ-ε) curves of stainless steel at elevated temperatures were defined on the basis of the two-stage compound Ramberg–Osgood material model [25–28] as given by eqs. (1) and (2):

$$\varepsilon = \frac{\sigma}{E_\theta} + 0.002\left(\frac{\sigma}{f_{\mathrm{p0.2},\theta}}\right)^{n_\theta} \quad \text{for} \quad \sigma \leq f_{\mathrm{p0.2},\theta} \tag{1}$$

$$\varepsilon = \frac{\sigma - f_{\mathrm{p0.2},\theta}}{E_{\mathrm{p0.2},\theta}} + \left(\varepsilon_{\mathrm{u},\theta} - \varepsilon_{\mathrm{p0.2},\theta} - \frac{f_{\mathrm{u},\theta} - f_{\mathrm{p0.2},\theta}}{E_{\mathrm{p0.2},\theta}}\right)\left(\frac{\sigma - f_{\mathrm{p0.2},\theta}}{f_{\mathrm{u},\theta} - f_{\mathrm{p0.2},\theta}}\right)^{m_\theta} + \varepsilon_{\mathrm{p0.2},\theta} \quad \text{for} \quad f_{\mathrm{p0.2},\theta} < \sigma \leq f_{\mathrm{u},\theta}, \tag{2}$$

where E_θ is the Young's modulus at temperature θ, $E_{\mathrm{p0.2},\theta}$ and $\varepsilon_{\mathrm{p0.2},\theta}$ are the tangent modulus and total strain corresponding to $f_{\mathrm{p0.2},\theta}$, respectively, $f_{\mathrm{u},\theta}$ and $\varepsilon_{\mathrm{u},\theta}$ are the ultimate tensile strength and strain at temperature θ, respectively, and n_θ and m_θ are the strain hardening exponents. The elevated temperature material strengths (the 0.2% proof strength $f_{\mathrm{p0.2},\theta}$, the strength at 2% total strain $f_{2,\theta}$, and $f_{\mathrm{u},\theta}$) and the elevated temperature ultimate strain ($\varepsilon_{\mathrm{u},\theta}$) in eqs. (1) and (2) were determined by multiplying the standardised room temperature material properties (f_y, f_u and ε_u) set out for hot-rolled austenitic, duplex and ferritic stainless steel plates [29] by the corresponding strength reduction factors ($k_{\mathrm{p0.2},\theta}$, $k_{2,\theta}$ and $k_{\mathrm{u},\theta}$) and ductility reduction factor ($k_{\varepsilon_{\mathrm{u},\theta}}$) given in [30], i.e. $f_{\mathrm{p0.2},\theta} = k_{\mathrm{p0.2},\theta} f_\mathrm{y}$, $f_{2,\theta} = k_{2,\theta} f_\mathrm{y}$, $f_{\mathrm{u},\theta} = k_{\mathrm{u},\theta} f_\mathrm{u}$, and $\varepsilon_{\mathrm{u},\theta} = k_{\varepsilon_{\mathrm{u},\theta}} \varepsilon_\mathrm{u}$. The elevated temperature Young's modulus E_θ was determined by multiplying the room temperature Young's modulus of 200 GPa with the stiffness reduction factor $k_{\mathrm{E},\theta}$ provided in [30]. The strain hardening exponent n_θ in eq. (1) was taken equal to its value at room temperature n as recommended in [30], while the strain hardening exponent m_θ in eq. (2) was calculated from:

$$m_\theta = \frac{\ln\left(\dfrac{0.02 - \varepsilon_{\mathrm{p0.2},\theta} - \dfrac{f_{2,\theta} - f_{\mathrm{p0.2},\theta}}{E_{\mathrm{p0.2},\theta}}}{\varepsilon_{\mathrm{u},\theta} - \varepsilon_{\mathrm{p0.2},\theta} - \dfrac{f_{\mathrm{u},\theta} - f_{\mathrm{p0.2},\theta}}{E_{\mathrm{p0.2},\theta}}}\right)}{\ln\left(\dfrac{f_{2,\theta} - f_{\mathrm{p0.2},\theta}}{f_{\mathrm{u},\theta} - f_{\mathrm{p0.2},\theta}}\right)}, \tag{3}$$

which ensures that the second stage of the Ramberg-Osgood material model passes through $f_{2,\theta}$ and $f_{\mathrm{u},\theta}$ exactly at 2% total strain and the ultimate strain $\varepsilon_{\mathrm{u},\theta}$ respectively [32]. The material model was inputted into ABAQUS in a multi-linear form by defining pairs of stress/strain points at 5 MPa intervals to ensure an accurate description of the rounded stress-strain response.

Residual stresses were incorporated into the finite element models by adopting the residual stress pattern proposed by Yuan et al. [33] for arc-welded stainless steel I-sections. As can be seen in Fig. 3, the peak tensile residual stresses in the flanges (σ_ft) and web (σ_wt) were taken as 80% of the room temperature yield strength f_y for the austenitic stainless steel I-sections (i.e. $\sigma_\mathrm{ft} = \sigma_\mathrm{wt} = 0.8 f_\mathrm{y}$), while the peak tensile residual stresses in the flanges and web were taken as 60% of the room temperature yield strength f_y for the duplex and ferritic stainless steel I-sections (i.e. $\sigma_\mathrm{ft} = \sigma_\mathrm{wt} = 0.6 f_\mathrm{y}$). The peak compressive residual stresses in the flanges (σ_fc) and web (σ_wc) were then calculated by considering the cross-section axial force equilibrium, as recommended in [33]. The residual stresses were incorporated into the FE models by defining stress values at the element integration points at room temperature; when the temperature of the FE models was increased, the residual stresses decreased with the development of thermal strains.

The finite element models were analysed isothermally by adopting the three steps followed in Kucukler et al. [34]. The first step, performed using a *STATIC, General analysis, was the application of the residual stresses in conjunction with the residual plastic strains $\varepsilon_\mathrm{res,pl}$, where the residual

plastic strains $\varepsilon_{\mathrm{res,pl}}$ were calculated considering the Ramberg–Osgood material model defined in eq. (1), where σ_{res} is the value of the applied residual stress at each location, as recommended in [35]:

$$\varepsilon_{\mathrm{res,pl}} = 0.002\left(\frac{\sigma_{\mathrm{res}}}{f_{\mathrm{y}}}\right)^{n}. \tag{4}$$

After reaching self-equilibrium in the first step, the temperature of the model was uniformly increased to the target temperature θ in the second step, performed using a *STATIC, General analysis, during which the development of thermal strains was allowed. Finally, the loading was applied in the third step, where the modified Riks analysis was utilised to trace the full load-deformation response of the stainless steel I-sections at the designated elevated temperature level θ. The Riks analysis adopted herein was load-controlled and hence the peak load obtained in this step was taken as the ultimate cross-section resistance of the I-sections at the designated elevated temperature value θ. The adopted modified Riks method used load increments with reasonable values for the initial increment (equal to 0.1), minimum increment size (equal to 10^{-15}) and maximum increment size (equal to 0.1), thus ensuring the attainment of a sufficient number increments before reaching the peak loads.

2.2. Validation of numerical models

The finite element models for stainless steel I-sections in compression were validated against the results of the fire tests performed on stainless steel box section stub columns in [36] and carbon steel I-section stub columns in [37] due to the absence of fire tests on stainless steel I-section stub columns in the literature. Validation of the finite element models for stainless steel I-sections in bending was carried out against the results obtained from the fire tests on I-sections under major axis bending conducted by Gardner and Baddoo [14] and under minor axis bending by Xing et al. [38].

2.2.1. Stainless steel I-sections in compression

Six fire tests on grade 1.4301 austenitic stainless steel square hollow section (SHS) stub columns carried out by Ala-Outinen and Oksanen [36] were utilised to validate the finite element modelling approach adopted in this paper. The geometric properties and local imperfections of the six stub columns reported in [36] were included in the finite element models created herein. Twenty elements were employed for each face of the SHS profiles; the element number along the member length was then determined to achieve an element aspect ratio of unity. The two-stage Ramberg-Osgood material model given in eqs. (1) and (2) was utilised to define the material response of the specimens at elevated temperatures, using the elevated temperature material properties determined by multiplying the strength and stiffness reduction factors given in [30] by the room temperature material properties obtained from the tensile coupon tests in [36]. The analysis steps described in Section 2.1 were adopted in the validation of the finite element models with the target temperature θ taken equal to the critical temperature θ_{cr} in the fire tests. The numerically determined failure loads $N_{\mathrm{u,FE}}$ are compared against those obtained from the tests $N_{\mathrm{u,test}}$ in Table 1, where it can be seen that the ratios of the numerically determined failure loads $N_{\mathrm{u,FE}}$ to those observed in the experiments $N_{\mathrm{u,test}}$ (i.e. $N_{\mathrm{u,FE}}/N_{\mathrm{u,test}}$) are generally close to unity, indicating that the

finite element models created in this study can replicate the local buckling response of stainless steel cross-sections in fire.

Additionally, three fire tests on carbon steel I-section stub columns performed in [37], which were conducted isothermally at three different elevated temperature levels (400 °C, 550 °C and 700 °C), were also used to validate the finite element models created in this study. The measured geometric properties and elevated temperature material properties of the tested specimens were included in the finite element models. Fig. 4 shows a comparison of the load versus end shortening curves determined from the experiments and those obtained from the FE models created in this study. As can be seen from the figure, there is a good correlation between the experimental and numerical load versus end shortening paths, which verifies the accuracy and suitability of the finite element modelling approach adopted in this paper for simulating the fire behaviour of cross-sections in compression.

2.2.2. Stainless steel I-sections in bending

Experimental data from the two major axis bending fire tests performed in [14] and the four minor axis bending fire tests performed in [38] on grade 1.4301 austenitic stainless steel I-sections were utilised to validate the adopted finite element modelling approach for stainless steel I-sections in bending. In the validation studies, only the parts of the beams under constant bending moments were modelled, with the bending moments applied at the two end cross-sections; this was consistent with the finite element models used in the parametric studies. The full elevated temperature stress-strain curves obtained from a series of isothermal elevated temperature tensile coupon tests in [14] were employed to model the elevated temperature material behaviour for the beam tests reported in [14], while the two-stage Ramberg-Osgood material model given by eqs. (1) and (2), using the elevated temperature material properties determined by multiplying the strength and stiffness reduction factors given in [30] by the room temperature material properties obtained from tensile coupon tests [38], was employed for the beam tests reported in [38]. Table 2 summarises the ultimate bending moment resistances obtained from the finite element analyses $M_{\mathrm{u,FE}}$ and those from the fire tests $M_{\mathrm{u,test}}$, where it can be seen that the numerical results are in a good agreement with the test results, thus verifying that the finite element modelling approach adopted in this study is also able to accurately capture the structural response of stainless steel I-sections in bending at elevated temperatures.

2.3. Parametric studies

Upon validation of the finite element models, comprehensive structural performance data on stainless steel I-sections at elevated temperatures were generated by means of extensive numerical parametric studies, considering different stainless steel grades (corresponding to the three groups – Austenitic I, Duplex II and Ferritic II, defined in [30, 31]), elevated temperature levels (200 °C, 400 °C, 600 °C and 800 °C), loading conditions and cross-section geometries. The austenitic, duplex and ferritic stainless steel grades falling into the Austenitic I, Duplex II and Ferritic II groups are provided in [30]; their room temperature and elevated temperature material properties are shown in Table 3 and Fig. 5. Three loading conditions, namely axial compression, major axis bending and minor axis bending, and three cross-section aspect ratios (i.e. $h/b = 1.0, 1.5$ and 2.0) were considered. Various thicknesses were employed for the flange and web plates to generate a wide

range of plate slenderness values for the web $\overline{\lambda}_{\mathrm{p,w}}$ and flange $\overline{\lambda}_{\mathrm{p,f}}$ plates. The web $\overline{\lambda}_{\mathrm{p,w}}$ and flange $\overline{\lambda}_{\mathrm{p,f}}$ plate slendernesses were calculated using:

$$\overline{\lambda}_{\mathrm{p,w}} = \sqrt{\frac{f_y}{\sigma_{\mathrm{cr,w}}}}, \tag{5}$$

$$\overline{\lambda}_{\mathrm{p,f}} = \sqrt{\frac{f_y}{\sigma_{\mathrm{cr,f}}}}, \tag{6}$$

where the local buckling stresses of the individual plates (i.e. $\sigma_{\mathrm{cr,w}}$ and $\sigma_{\mathrm{cr,f}}$) were calculated from:

$$\sigma_{\mathrm{cr}} = k_\sigma \frac{\pi^2 E}{12(1-\nu^2)} \left(\frac{t}{b}\right)^2, \tag{7}$$

in which k_σ is the buckling coefficient determined for the corresponding boundary conditions and stress distribution of the plate [24], b is the plate width, t is the plate thickness and ν is the Poisson's ratio. The considered web $\overline{\lambda}_{\mathrm{p,w}}$ and flange $\overline{\lambda}_{\mathrm{p,f}}$ plate slenderness values are provided in Table 4, where it can be seen that I-sections with the web $\overline{\lambda}_{\mathrm{p,w}}$ and flange $\overline{\lambda}_{\mathrm{p,f}}$ plate slendernesses ranging from 0.15 to 2.0 were modelled. To expand the numerical data pool, in addition to the basic I-sections with the same web plate $\overline{\lambda}_{\mathrm{p,w}}$ and flange plate $\overline{\lambda}_{\mathrm{p,f}}$ slendernesses (i.e. $\overline{\lambda}_{\mathrm{p,w}} = \overline{\lambda}_{\mathrm{p,f}}$), two additional cases were also considered: (i) stainless steel I-sections with the web plate slendernesses $\overline{\lambda}_{\mathrm{p,w}}$ less than the flange plate slendernesses $\overline{\lambda}_{\mathrm{p,f}}$ (i.e. $\overline{\lambda}_{\mathrm{p,w}} < \overline{\lambda}_{\mathrm{p,f}}$) and (ii) stainless steel I-sections with the web plate slendernesses $\overline{\lambda}_{\mathrm{p,w}}$ greater than the flange plate slendernesses $\overline{\lambda}_{\mathrm{p,f}}$ (i.e. $\overline{\lambda}_{\mathrm{p,w}} > \overline{\lambda}_{\mathrm{p,f}}$). The flange and web thicknesses of the I-sections with $\overline{\lambda}_{\mathrm{p,w}}$ equal to $\overline{\lambda}_{\mathrm{p,f}}$ are shown in Table 5, where it can be seen that the web thicknesses were varied from 0.5 mm to 10 mm and the flange thickness were varied between 1.5 mm and 25 mm in the parametric studies.

Typical failure modes from the FE models under different loading conditions are shown in Fig. 6. As can be seen from Fig. 6 (a), there is local buckling in both web and two flanges of the I-sections under axial compression, while, as expected, for the I-sections in bending (see Figs. 6 (b) and (c)), local buckling is largely restricted to the portions of cross-sections under compressive stresses.

3. EN 1993-1-2 [11] rules for the design of stainless steel I-sections in fire

3.1. Cross-section classification

According to the current version of EN 1993-1-2 [11], stainless steel I-sections in fire are classified following the same rules as set out in EN 1993-1-4 [6] for room temperature design but using a reduced material factor ε_θ referred to herein as the elevated temperature material factor. The elevated temperature material factor ε_θ is defined in terms of the room temperature material factor ε through eq. (8).

$$\varepsilon_\theta = 0.85\varepsilon = 0.85\left[\frac{235}{f_{\mathrm{y}}}\frac{E}{210000}\right]^{0.5} \quad \text{with } f_{\mathrm{y}} \text{ and } E \text{ in MPa.} \tag{8}$$

Thus, stainless steel I-sections in fire are grouped into four classes; the class of the cross-section is taken as the highest class of its constituent plates. Table 6 summarises the specific width-to-thickness limit ratios provided in EN 1993-1-4 [6] used to determine the classes of the constituent internal and outstand plates of stainless steel sections at room temperature.

3.2. Effective width method

EN 1993-1-2 [11] states that the effective section properties for Class 4 sections should be determined as for room temperature design using the room temperature material factor ε; thus, the effective section properties of stainless steel members with Class 4 cross-sections at elevated temperatures are the same as those at room temperature. EN 1993-1-4 [6] provides a series of formulae for the calculation of the effective section properties of stainless steel I-sections at room temperature, where the plate buckling reduction factor ρ is calculated as:

$$\rho = \frac{0.772}{\overline{\lambda}_{\mathrm{p}}} - \frac{0.079}{\overline{\lambda}_{\mathrm{p}}^{\,2}} \quad \text{but} \quad \rho \leq 1.0 \tag{9}$$

for internal elements (i.e. the webs of stainless steel I-sections), while the plate buckling reduction factor ρ is calculated as:

$$\rho = \frac{1}{\overline{\lambda}_{\mathrm{p}}} - \frac{0.188}{\overline{\lambda}_{\mathrm{p}}^{\,2}} \quad \text{but} \quad \rho \leq 1.0 \tag{10}$$

for outstand elements (i.e. the flanges of stainless steel I-sections), in which the non-dimensional plate slenderness $\overline{\lambda}_{\mathrm{p}}$ is given by:

$$\overline{\lambda}_{\mathrm{p}} = \sqrt{\frac{f_{\mathrm{y}}}{\sigma_{\mathrm{cr}}}} = \frac{b/t}{28.4\varepsilon\sqrt{k_\sigma}}, \tag{11}$$

where σ_{cr} is the elastic buckling stress of the web or flange, b and t are the width and thickness of the web or flange plates, and k_σ is the plate buckling coefficient defined in EN 1993-1-5 [24].

3.3. Cross-section resistances

Table 7 summarises the resistances assigned to stainless steel cross-sections of different classes in fire, where $N_{\mathrm{fi,t,Rd}}$ and $M_{\mathrm{fi,t,Rd}}$ are the design cross-section axial and bending moment resistances in fire at time t, A and A_{eff} are the gross and effective cross-section areas, W_{pl}, W_{el} and W_{eff} refer to the plastic, elastic, and effective section moduli, respectively, $f_{2,\theta}$ is the elevated temperature material strength at 2% total strain, $f_{\mathrm{p0.2},\theta}$ is the elevated temperature 0.2% proof strength and $\gamma_{M,\mathrm{fi}}$ is the partial safety factor for fire design. The cross-section resistances are also graphically illustrated in Fig. 7. Since the elevated temperature strength at 2% total strain $f_{2,\theta}$ is utilised for Class 1–3 sections but the elevated temperature 0.2% proof strength $f_{\mathrm{p0.2},\theta}$ is utilised for Class 4 sections, there exists an abrupt step in the cross-section resistances at the transition between Class 3 and 4 sections, as shown in Fig. 7 (a) and (b). An abrupt step also exist in the bending moment resistances at the transition between Class 2 and 3 sections owing to the use of the plastic and elastic cross-section bending moment resistances respectively, as shown in Fig. 7 (b).

3.4. Assessment of EN 1993-1-2 [11] provisions for the cross-section design of stainless steel I-sections in fire

In this subsection, the accuracy of the current EN 1993-1-2 [11] design provisions for calculating the cross-section resistance of stainless steel I-section profiles in fire is assessed against the nonlinear shell finite element model results generated in Section 2.3. The assessment is presented in Fig. 8 for the austenitic stainless steel I-sections, in Fig. 9 for the duplex stainless steel I-sections and in Fig. 10 for the ferritic stainless steel I-sections. In these figures, $N_{\mathrm{u,FE}}$ and $M_{\mathrm{u,FE}}$ are the cross-section compression and bending moment resistances obtained from the FE simulations, while $N_{\mathrm{fi,Rd,EC3}}$ and $M_{\mathrm{fi,Rd,EC3}}$ are the cross-section compression and bending moment resistances predicted using EN 1993-1-2 [11]. As can be seen from the figures, EN 1993-1-2 [11] provides somewhat conservative ultimate resistance predictions for stainless steel I-sections under compression and major axis bending when the slendernesses of the constituent plates are high, while the predictions lie on the unsafe side in the intermediate slenderness range. For stainless steel I-sections in minor axis bending, the EN 1993-1-2 [11] resistance predictions become increasingly conservative with increasing slenderness and become very conservative in the slender range. This is because although the minor axis bending resistance of slender I-sections is determined on the basis of a linear elastic stress distribution acting over an effective cross-section, in reality significant inelastic behaviour, resulting in higher bending capacity, is observed. Note that, for clarity, the results shown in Figs. 8, 9 and 10 are for the I-sections with the same web $\overline{\lambda}_{\mathrm{p,w}}$ and flange $\overline{\lambda}_{\mathrm{p,f}}$ plate slendernesses (i.e. $\overline{\lambda}_{\mathrm{p,w}} = \overline{\lambda}_{\mathrm{p,f}}$); the full set of results are presented in Section 5.

4. Design method of [1] for stainless steel I-sections in fire

4.1. Cross-section classification

According to the design method proposed in [1], the four cross-section classes of EN 1993-1-2 [11] are replaced with two cross-section classes, referred to as 'non-slender' and 'slender'. As usual, the overall cross-section class is determined on the basis of the most slender constituent plate element. The plateau slenderness $\overline{\lambda}_{\mathrm{p0},\theta}$ denotes the transition between 'non-slender' and 'slender' cross-sections. Plate elements with local slendernesses less than or equal to the plateau slenderness $\overline{\lambda}_{\mathrm{p0},\theta}$ (i.e. $\overline{\lambda}_{\mathrm{p},\theta} \leq \overline{\lambda}_{\mathrm{p0},\theta}$) are classified as 'non-slender', while those with local slendernesses greater than the plateau slenderness $\overline{\lambda}_{\mathrm{p0},\theta}$ (i.e. $\overline{\lambda}_{\mathrm{p},\theta} > \overline{\lambda}_{\mathrm{p0},\theta}$) are classified as 'slender'. The plateau slenderness values $\overline{\lambda}_{\mathrm{p0},\theta}$ for internal and outstand elements are given in Section 4.2 and differ between austenitic, duplex and ferritic stainless steels.

4.2. Effective width method

New effective width formulae were proposed in [1] for the local buckling assessment of slender stainless steel cross-sections in fire. According to the new method, the local buckling reduction factor ρ is equal to unity for all non-slender plates:

$$\rho = 1 \qquad \text{for} \quad \overline{\lambda}_{\mathrm{p},\theta} \leq \overline{\lambda}_{\mathrm{p0},\theta}. \tag{12}$$

For slender internal elements in austenitic stainless steel sections, the local buckling reduction factor ρ is given by:

$$\rho = \frac{0.54}{\left(\overline{\lambda}_{\mathrm{p},\theta}/\sqrt{\xi_\theta}\right)^{0.75}} - \frac{0.015\,(3+\psi)}{\left(\overline{\lambda}_{\mathrm{p},\theta}/\sqrt{\xi_\theta}\right)^{1.5}} \quad \text{for} \quad \overline{\lambda}_{\mathrm{p},\theta} > \overline{\lambda}_{\mathrm{p0},\theta}, \tag{13}$$

with

$$\overline{\lambda}_{\mathrm{p0},\theta} = \left(0.27 + \sqrt{0.0279 - 0.015\psi}\right)^{1.33} \sqrt{\xi_\theta}, \tag{14}$$

where $\overline{\lambda}_{\mathrm{p},\theta}$ is the elevated temperature plate slenderness expressed as:

$$\overline{\lambda}_{\mathrm{p},\theta} = \xi_\theta \sqrt{\frac{f_\mathrm{y}}{\sigma_\mathrm{cr}}} \quad \text{with} \quad \xi_\theta = \sqrt{\frac{k_{2,\theta}}{k_{E,\theta}}} \tag{15}$$

and $\psi = \sigma_2/\sigma_1$ is the ratio between the stresses at the two edges of the plate, where σ_1 is the maximum compressive stress (with compression positive) and σ_2 is the minimum compressive stress or maximum tensile stress, as defined in EN 1993-1-5 [24]. For slender internal elements in duplex and ferritic stainless steel sections, the local buckling reduction factor ρ is given by:

$$\rho = \frac{0.6}{\left(\overline{\lambda}_{\mathrm{p},\theta}/\sqrt{\xi_\theta}\right)^{0.75}} - \frac{0.015\,(3+\psi)}{\left(\overline{\lambda}_{\mathrm{p},\theta}/\sqrt{\xi_\theta}\right)^{1.5}} \quad \text{for} \quad \overline{\lambda}_{\mathrm{p},\theta} > \overline{\lambda}_{\mathrm{p0},\theta}, \tag{16}$$

with

$$\overline{\lambda}_{\mathrm{p0},\theta} = \left(0.3 + \sqrt{0.045 - 0.015\psi}\right)^{1.33} \sqrt{\xi_\theta}. \tag{17}$$

For slender outstand flanges in austenitic stainless steel sections, the local buckling reduction factor ρ is calculated as:

$$\rho = \frac{0.6}{\left(\overline{\lambda}_{\mathrm{p},\theta}/\sqrt{\xi_\theta}\right)^{0.6}} - \frac{0.075}{\left(\overline{\lambda}_{\mathrm{p},\theta}/\sqrt{\xi_\theta}\right)^{1.2}} \quad \text{for} \quad \overline{\lambda}_{\mathrm{p},\theta} > \overline{\lambda}_{\mathrm{p0},\theta}, \tag{18}$$

with

$$\overline{\lambda}_{\mathrm{p0},\theta} = 0.237 \sqrt{\xi_\theta}, \tag{19}$$

while for slender outstand flanges in duplex and ferritic stainless steel sections, the local buckling reduction factor ρ is given by:

$$\rho = \frac{0.67}{\left(\overline{\lambda}_{\mathrm{p},\theta}/\sqrt{\xi_\theta}\right)^{0.6}} - \frac{0.075}{\left(\overline{\lambda}_{\mathrm{p},\theta}/\sqrt{\xi_\theta}\right)^{1.2}} \quad \text{for} \quad \overline{\lambda}_{\mathrm{p},\theta} > \overline{\lambda}_{\mathrm{p0},\theta}, \tag{20}$$

with

$$\overline{\lambda}_{\mathrm{p0},\theta} = 0.344 \sqrt{\xi_\theta}. \tag{21}$$

4.3. Cross-section resistances

The determination of the cross-section resistances of stainless steel I-sections falling into the 'non-slender' and 'slender' classes is shown in Table 8 and Fig. 11. As can be seen from Fig. 11, only one reference strength – the elevated temperature strength at 2% total strain $f_{2,\theta}$ – is adopted in the new proposal so as to avoid the discontinuity resulting from the use of different reference strengths at the transition between Class 3 and Class 4 sections in EN 1993-1-2 [11]. The same approach was proposed in [39–42] for the design of carbon steel cross-sections at elevated temperatures.

4.4. Assessment of the design method of [1] for stainless steel I-sections in fire

The accuracy of the design method developed in [1] for the prediction of the cross-section response of stainless steel I-sections in fire is investigated in this section. Comparisons between the FE results and design predictions are presented in Figs. 12–14 for austenitic, duplex and ferritic stainless steel I-sections, respectively, where $N_{\mathrm{fi,Rd,prop}}$ and $M_{\mathrm{fi,Rd,prop}}$ are the elevated temperature cross-section compression and bending moment resistances predicted using the design method of [1]. As can be seen from the figures, relative to EN 1993-1-2 [11], the design method of [1] provides more consistent resistance predictions for the cases of axial compression and major axis bending with no results on the unsafe side. This is because the influence of the variation of strength and stiffness at different elevated temperature levels is appropriately captured [1]. For the case of stainless steel I-sections under minor axis bending, similar to EN 1993-1-2 [11], the predictions of the design method of [1] are overly conservative; again, this results from the neglect of the inelastic behaviour of outstand flanges under stress gradients. To address this overconservatism, the plastic effective width method of [2], which was originally developed to reflect the room temperature inelastic behaviour of outstand flanges under stress gradients within carbon steel I-sections, is extended herein to the prediction of the minor axis bending moment resistance of stainless steel I-sections at elevated temperatures, as presented in the following section.

4.5. Extension of the plastic effective width method of [2] to the design of stainless steel I-sections under minor axis bending in fire

In the plastic effective width method of Bambach and Rasmussen [2], the effective width of outstand flanges under stress gradients is assumed to be located at an eccentricity relative to the supported edge and hence two variables – effective width b_{eff} and eccentricity e_1 – are utilised as shown in Fig. 15. Adopting the elevated temperature plate buckling slenderness $\overline{\lambda}_{\mathrm{p},\theta}$ defined in eq. (15), the effective width b_{eff} of the flanges of I-sections subjected to minor axis bending can be calculated by [2]:

$$\frac{b_{\mathrm{eff}}}{b} = 0.4(1+\psi)\overline{\lambda}_{\mathrm{p},\theta}^{\,-\frac{3}{4}} \leq 1 \tag{22}$$

and eccentricity e_1 is given by [2]:

$$e_1 = 0.45b(1-\psi) \leq 1 - \frac{b_{\mathrm{eff}}}{b} \quad \text{for } 0 \leq \psi \leq 1, \tag{23}$$

where ψ is the ratio of the stresses at the plate edges. Once b_{eff} and e_1 have been calculated, the strain distribution can be determined on the assumption that the maximum allowable strain in the

effective section is equal to three times the yield strain (i.e. $\varepsilon_{max} = 3\varepsilon_y$), as illustrated in Fig. 15 (a); the corresponding stress distribution, where the stress σ is equal to f_y ($\sigma = f_y$) when the strain is greater than or equal to ε_y ($\varepsilon \geq \varepsilon_y$) while the stress σ is equal to εE_θ when the strain is less than ε_y ($\varepsilon < \varepsilon_y$), is shown in Fig. 15 (b). The moment capacity of the cross-section is then determined based on the resulting stress distribution. The accuracy of the plastic effective width method of [2], with the plate slenderness of [1], is assessed in Fig. 16, where it can be seen that the ratios of the minor axis bending moment resistances to those obtained from the shell finite element models are generally close to unity, demonstrating the suitability of the plastic effective width method for the design of stainless steel I-sections under minor axis bending at elevated temperatures.

5. Comparison of design methods and reliability assessment

In this section, the accuracy and reliability of the design methods of Xing et al. [1] and Bambach and Rasmussen [2], as well as EN 1993-1-2 [11], for determining the cross-section resistance of stainless steel I-sections in fire are assessed. Comparisons are made against a total of over 1000 shell FE results covering different stainless steel grades, elevated temperature levels, loading conditions and cross-section geometries against those of the existing design rules in EN 1993-1-2 [11]. For design using the methods set out in [1, 2], the Xing et al. [1] expressions alone were used for the cases of axial compression and major axis bending, while the Bambach and Rasmussen [2] expressions, with the Xing et al. [1] plate slenderness definition, were used for minor axis bending.

5.1. Accuracy assessment

The accuracy of the design methods of Xing et al. [1] and Bambach and Rasmussen [2] is visually illustrated against that of the existing design rules of EN 1993-1-2 [11] in Fig. 17. Four different elevated temperature levels ranging from 200 °C to 800 °C in increments of 200 °C and the range of local plate slenderness values listed in Table 4 were considered. As can be seen from the figure, the design methods of Xing et al. [1] and Bambach and Rasmussen [2] lead to more accurate and consistent cross-section resistance predictions relative to the existing design rules of EN 1993-1-2 [11], particularly for I-sections subjected to minor axis bending. In Table 9, the accuracy of the design methods of Xing et al. [1] and Bambach and Rasmussen [2] is assessed in terms of the mean value and the coefficient of variation (COV) of the ratios of the cross-section resistances obtained from the numerical simulations to the corresponding predictions determined using the design methods of [1, 2] (i.e. $\varepsilon = N_{u,FE}/N_{fi,Rd,prop}$). As can be seen from Table 9, relative to EN 1993-1-2 [11], the design methods of Xing et al. [1] and Bambach and Rasmussen [2] provide more accurate and safe-sided cross-section resistance predictions with a lower level of scatter, indicating the better suitability of these methods for the design of stainless steel I-sections in fire.

5.2. Reliability assessment

The reliability of the methods provided in EN 1993-1-2 [11] and [1, 2] for the cross-section design of stainless steel I-sections in fire is assessed by considering the three reliability criteria proposed by Kruppa [44] in this subsection. The first criterion of [44] states that the ultimate resistances predicted by a design method should not exceed the numerical results by more than 15%;

the second criterion of [44] states that the percentage of the design predictions on the unsafe side should be less than 20%, and the third criterion of [44] states that the design predictions should be safe-sided, on average. The reliability assessment of the design methods given in EN 1993-1-2 [11] and [1, 2] are summarised in Table 10, where Criterion 1 refers to the percentage of the strength predictions that exceed the corresponding numerical predictions by more than 15%, Criterion 2 refers to the percentage of the design predictions on the unsafe side and Criteria 3 refers to the average percentage difference between the design predictions and numerical results, with negative values indicating that the capacity predictions are safe-sided on average. The violated criteria are marked with '*'. As can be seen from the table, EN 1993-1-2 [11] frequently violates the reliability criteria of [44], while the design methods of Xing et al. [1] and Bambach and Rasmussen [2] satisfy all the criteria of [44], indicating their suitability for the design of stainless steel I-sections in fire.

6. Conclusions

The cross-section behaviour and design of stainless steel I-sections in fire have been investigated in this paper. To simulate the response of stainless steel I-sections at elevated temperatures, shell finite element models were created and validated against a series of experimental results from the literature. Parametric studies were then carried out, in which different cross-section geometries, stainless steel grades, elevated temperature levels and loading conditions were considered. The design methods provided in the current version of EN 1993-1-2 [11] and by Xing et al. [1] were subsequently assessed against the numerical results from the parametric studies, where shortcomings of the existing rules in EN 1993-1-2 [11] for the design of stainless steel I-sections in fire have been highlighted. Unlike EN 1993-1-2 [11], the design guidance of Xing et al. [1] was shown to provide accurate predictions of the response of stainless steel I-sections under compression and major axis bending in fire owing to the adoption of a new cross-section classification approach in conjunction with the temperature-dependent local buckling curves. Moreover, to consider the inelastic behaviour of slender outstand flanges under stress gradients, which was observed for stainless steel I-sections under minor axis bending, the plastic effective width method of [2], originally developed for the room temperature design of carbon steel I-sections, was extended to the design of stainless steel I-sections under minor axis bending in fire. The present research demonstrated the accuracy and reliability of the design methods of Xing et al. [1] and Bambach and Rasmussen [2] for stainless steel I-sections in fire, and confirmed the suitability of the design method of [1] for inclusion into the upcoming version of 1993-1-2 [11].

References

[1] Xing, Z., Kucukler, M. and Gardner, L.. Local buckling of stainless steel plates in fire. Thin-Walled Structures 2020;148,106570.

[2] Bambach, M.R. and Rasmussen, K.J.. Effective widths of unstiffened elements with stress gradient. Journal of Structural Engineering 2004;130(10):1611–1619.

[3] Kucukler, M., Gardner, L. and Bu, Y.. Flexural-torsional buckling of stainless steel I-section beam-columns: Testing, numerical modelling and design. Thin-Walled Structures 2020;150,16572.

[4] Sun, Y., Liang, Y. and Zhao, O.. Local–flexural interactive buckling behaviour and resistances of high-chromium stainless steel slender welded I-section columns. Engineering Structures 2020;220:111022.

[5] Sun, Y., He, A., Liang, Y. and Zhao, O.. Flexural buckling behaviour of high-chromium stainless steel welded I-section columns. Thin-Walled Structures 2020;154:106812.
[6] EN 1993-1-4, Eurocode 3 Design of steel structures–Part 1-4: General rules–Supplementary rules for stainless steels. European Committee for Standardization (CEN), Brussels; 2015.
[7] Johnson A.L. and Winter G. The structural performance of austenitic stainless steel members (Report no. 327). Department of Structural Engineering, School of Civil Engineering, Cornell University; 1966.
[8] Wang S.T. and Winter G.. Cold rolled austenitic stainless steel: Material properties and structural performance (Report no. 334). Dept. of Structural Engineering, Cornell University; 1969.
[9] Yamada S., Kurino H. and Kato B.. Ultimate strength of H-shaped stub-columns of stainless steel. In: Proceedings of the Institute of Architects; 1988.
[10] Kuwamura H.. Local buckling consideration in design of thin-walled stainless steel members. Lecture at Pusan National University; 2001.
[11] EN 1993-1-2, Eurocode 3 Design of Steel Structures–Part 1-2: General Rules–Structural Fire Design. European Committee for Standardization (CEN), Brussels; 2005.
[12] He, A., Liang, Y. and Zhao, O.. Experimental and numerical studies of austenitic stainless steel CHS stub columns after exposed to elevated temperatures. Journal of Constructional Steel Research 2019;154:293-305.
[13] Su, A., Sun, Y., Liang, Y. and Zhao, O.. Material properties and membrane residual stresses of S690 high strength steel welded I-sections after exposure to elevated temperatures. Thin-Walled Structures 2020;152:106723.
[14] Gardner, L. and Baddoo, N.. Fire testing and design of stainless steel structures. Journal of Constructional Steel Research 2006;62:532–543.
[15] Lopes, N., Vila-Real, P., Da Silva, L.S. and Franssen, J.M.. Numerical modelling of thin-walled stainless steel structural elements in case of fire. Fire Technology 2010;46(1):91.
[16] Rusch, A. and Lindner, J.. Application of level 1 interaction formulae to class 4 sections. Thin-walled structures 2014;42(2):279–293.
[17] ABAQUS v.6.14 Reference Manual. Simulia, Dassault Systemes; 2014.
[18] Kucukler, M., Gardner, L. and Macorini, L.. Flexural-torsional buckling assessment of steel beam-columns through a stiffness reduction method. Engineering Structures 2015;101:662–676.
[19] Kucukler, M., Gardner, L. and Macorini, L.. Lateral-torsional buckling assessment of steel beams through a stiffness reduction method. Journal of Constructional Steel Research 2015;109:87–100.
[20] Sun, Y. and Zhao, O.. Material response and local stability of high-chromium stainless steel welded I-sections. Engineering Structures 2019;178:212–226.
[21] Liang, Y., Jeyapragasam, V.V.K., Zhang, L. and Zhao, O.. Flexural-torsional buckling behaviour of fixed-ended hot-rolled austenitic stainless steel equal-leg angle section columns. Journal of Constructional Steel Research 2019;154:43–54.
[22] Kucukler, M.. Compressive resistance of high-strength and normal-strength steel CHS members at elevated temperatures. Thin-Walled Structures 2020;152:106753.
[23] Kucukler, M.. Lateral instability of steel beams in fire: Behaviour, numerical modelling and design. Journal of Constructional Steel Research 2020;170:106095.
[24] EN 1993-1-5, Eurocode 3 Design of steel structures-Part 1-5: Plated structural elements, European Committee for Standardization (CEN), Brussels; 2005.
[25] Arrayago, I., Real, E. and Gardner, L.. Description of stress-strain curves for stainless steel alloys. Materials and Design 2015;87:540–552.
[26] Gardner, L. and Yun, X.. Description of stress-strain curves for cold-formed steels. Construction and Building Materials 2018;189:527–538.
[27] Mirambell, E. and Real, E.. On the calculation of deflections in structural stainless steel beams: an experimental and numerical investigation. Journal of Constructional Steel Research 2000;54(1):109–133.
[28] Rasmussen, K.J.. Full-range stress-strain curves for stainless steel alloys. Journal of Constructional Steel Research 2003;59(1):47–61.
[29] Afshan, S., Zhao, O. and Gardner, L.. Standardised material properties for numerical parametric studies of stainless steel structures and buckling curves for tubular columns. Journal of Constructional Steel Research 2009;152:2–11.

[30] Design Manual for Structural Stainless Steel, Fourth Edition, Steel Construction Institute (SCI); 2017.
[31] Gardner, L., Insausti, A., Ng, K., Ashraf, M.. Elevated temperature material properties of stainless steel alloys. Journal of Constructional Steel Research 2010;66:634–647.
[32] Liang, Y., Manninen, T., Zhao, O., Walport, F. and Gardner, L.. Elevated temperature material properties of a new high-chromium austenitic stainless steel, Journal of Constructional Steel Research 2019;152:261–273.
[33] Yuan, H., Wang, Y., Shi, Y. and Gardner, L.. Residual stress distributions in welded stainless steel sections. Thin-Walled Structures 2014;79:38–51.
[34] Kucukler, M., Xing, Z. and Gardner, L.. Behaviour and design of stainless steel I-section columns in fire, Journal of Constructional Steel Research 2020;165,105890.
[35] Jandera, M., Gardner, L. and Machacek, J.. Residual stresses in cold-rolled stainless steel hollow sections. Journal of Constructional Steel Research 2008;64(11):1255-1263.
[36] Ala-Outinen, T. and Oksanen, T.. Stainless steel compression members exposed to fire, Research Notes 1864, Technical Research Centre of Finland (VTT), Finland; 1997.
[37] Pauli, J.. The behaviour of steel columns in fire: material – cross-sectional capacity – column buckling. IBK Bericht 2012;343.
[38] Xing, Z., Zhao O., Kucukler, M. and Gardner, L.. Testing and design of slender stainless steel I-sections in minor axis bending in fire. Engineering Structures 2020;Submitted for publication.
[39] Franssen, J.M., Morente, F., Vila Real, P., Wald, F., Sanzel, A. and Zhao, B.. Fire design of steel members with welded or hot-rolled class 4 cross-sections (FIDESC4). Luxembourg: Publications Office; 2016.
[40] Couto, C., Vila Real, P., Lopes, N. and Zhao, B.. Effective width method to account for the local buckling of steel thin plates at elevated temperatures. Thin-Walled Structures 2014;84:134–149.
[41] Couto, C., Vila Real, P., Lopes, N. and Zhao, B.. Resistance of steel cross-sections with local buckling at elevated temperatures. Journal of Constructional Steel Research 2015;109:101–114.
[42] Couto, C., Vila Real, P., Lopes, N. and Zhao, B.. Local buckling in laterally restrained steel beam-columns in case of fire. Journal of Constructional Steel Research 2016;122:543–556.
[43] Bambach, M.R., Rasmussen, K.J. and Ungureanu, V.. Inelastic behaviour and design of slender I-sections in minor axis bending. Journal of Constructional Steel Research 2007;63(1):1–12.
[44] Kruppa, J.. Eurocodes-fire parts: Proposal for a methodology to check the accuracy of assessment methods. CEN TC 250, Horizontal Group Fire, Document no: 99/130; 1999.

7. Figures

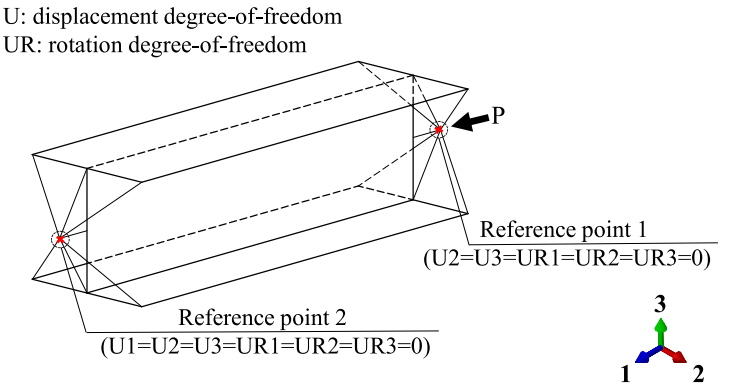

(a) I-sections in compression

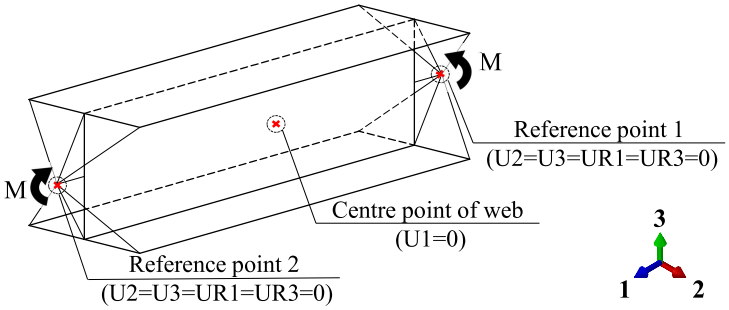

(b) I-sections in bending about the major axis

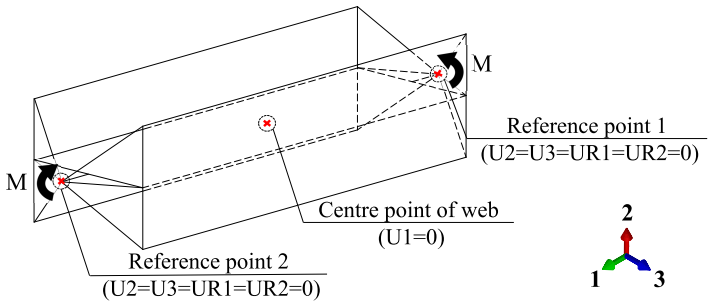

(c) I-sections in bending about the minor axis

Figure 1: Boundary conditions applied to the finite element models

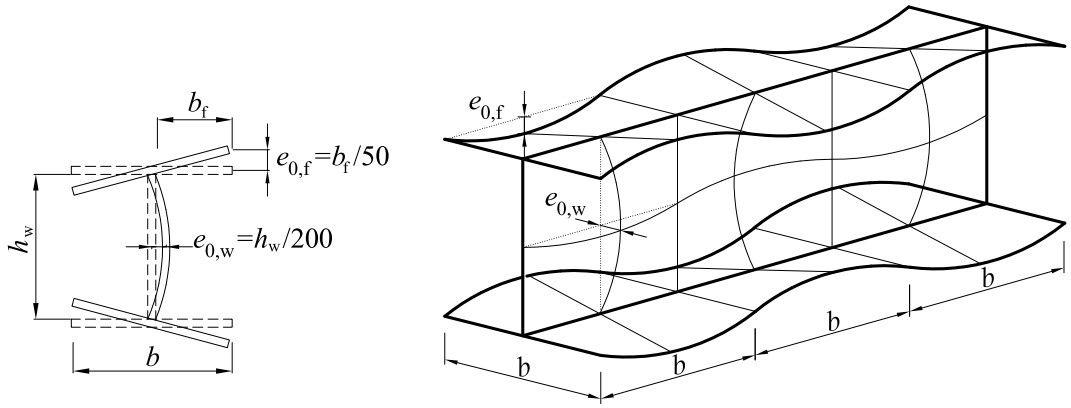

Figure 2: Local imperfections applied to the finite element models

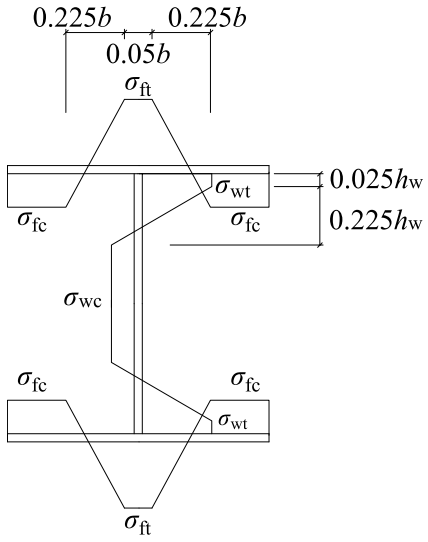

Figure 3: Residual stress patterns applied to the finite element models

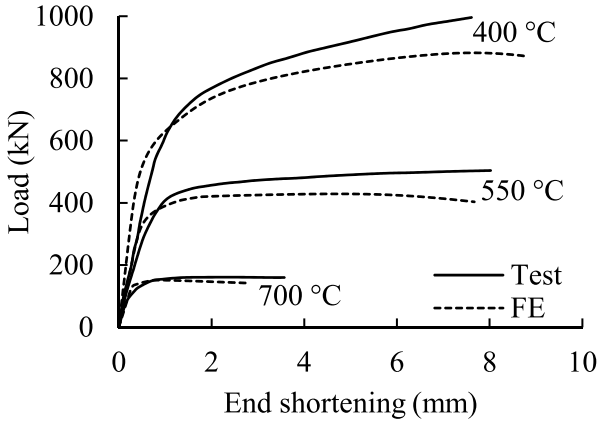

Figure 4: Comparison between load versus end shortening curves obtained from experiments [37] and finite element models for carbon steel I-section stub columns in fire

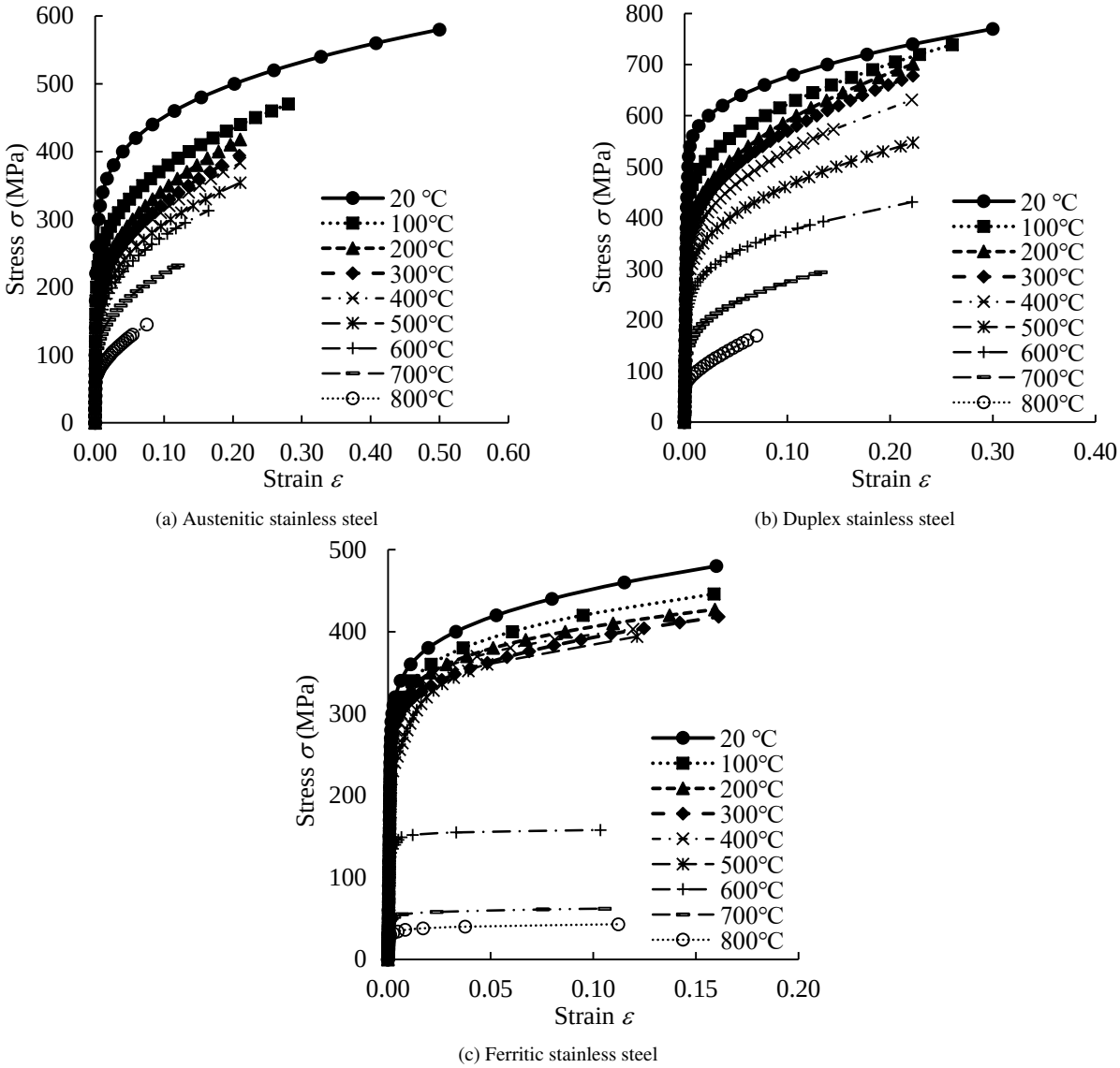

(a) Austenitic stainless steel

(b) Duplex stainless steel

(c) Ferritic stainless steel

Figure 5: Stress-strain response of different stainless steel grades at elevated temperatures

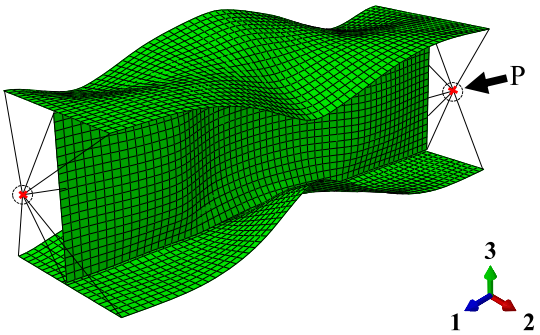

(a) I-sections in compression

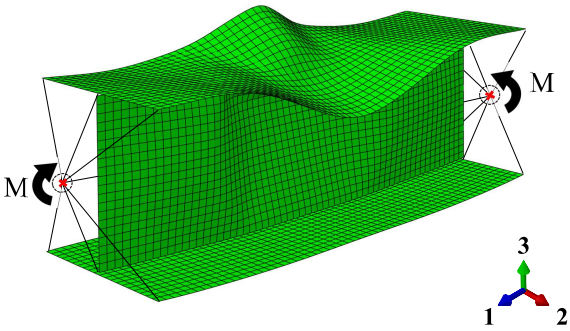

(b) I-sections in bending about the major axis

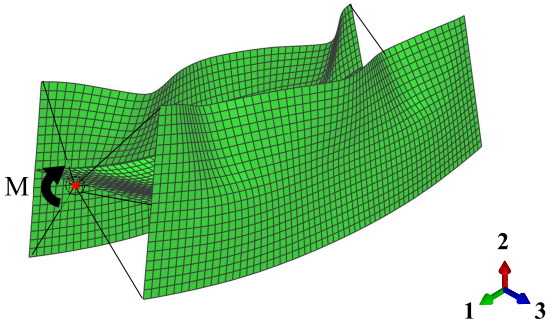

(c) I-sections in bending about the minor axis

Figure 6: Typical failure modes of stainless steel I-sections under different loading conditions

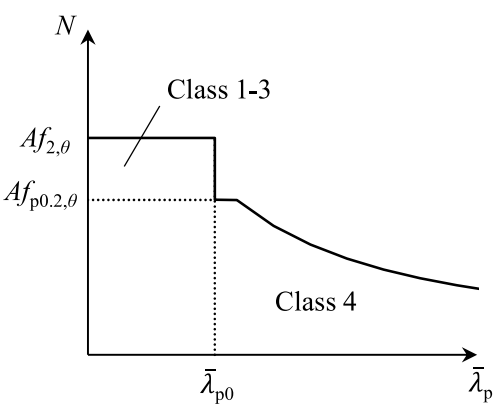

(a) Stainless steel I-sections in compression

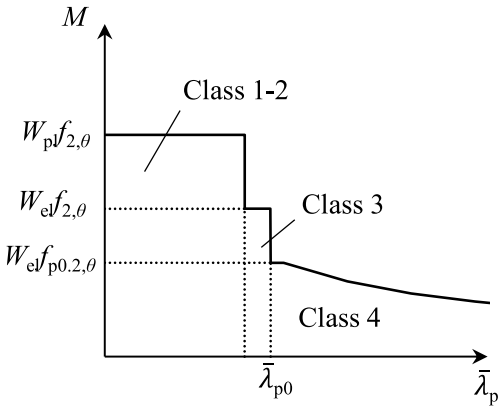

(b) Stainless steel I-sections in bending

Figure 7: Illustration of cross-section resistances in EN 1993-1-2 [11]

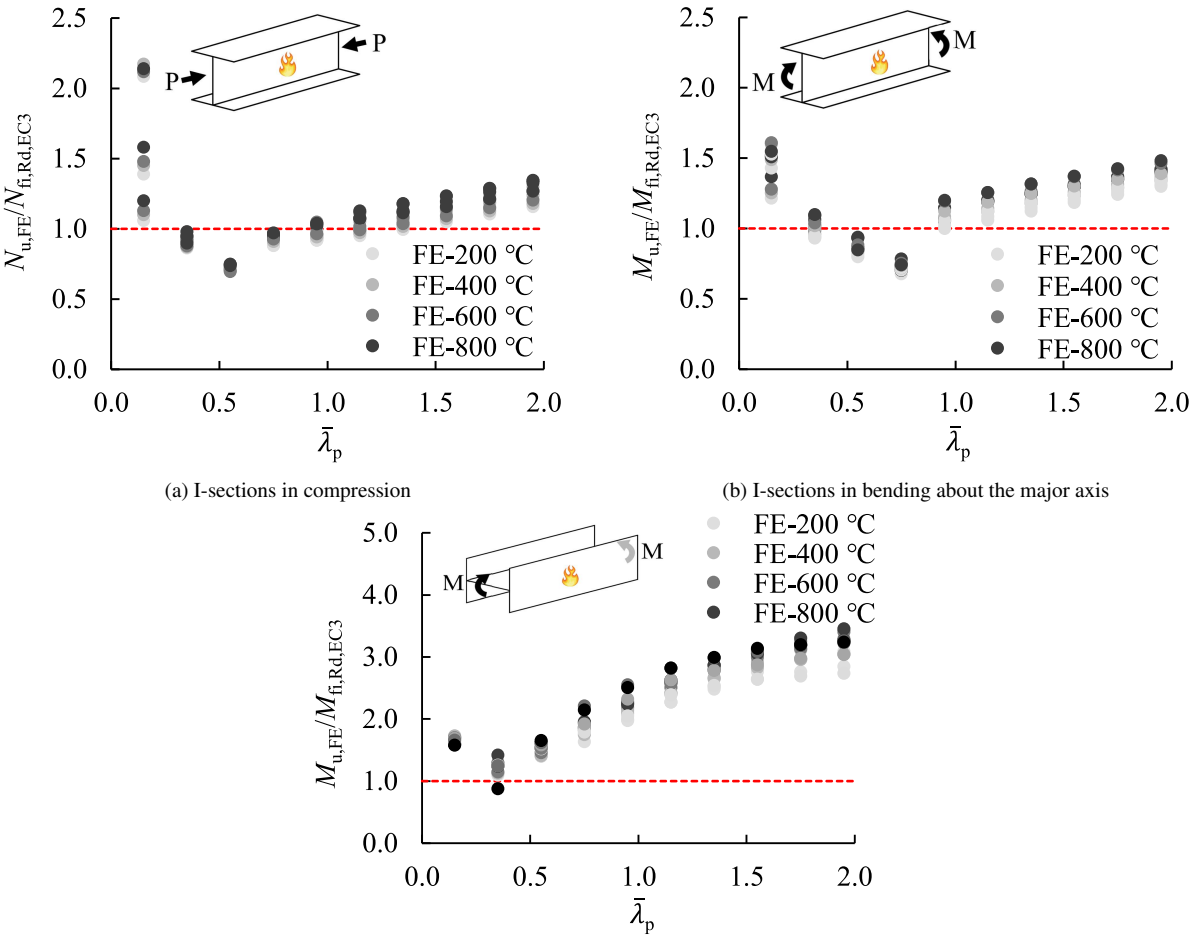

(a) I-sections in compression

(b) I-sections in bending about the major axis

(c) I-sections in bending about the minor axis

Figure 8: Assessment of EN 1993-1-2 [11] against FE results for austenitic stainless steel I-sections

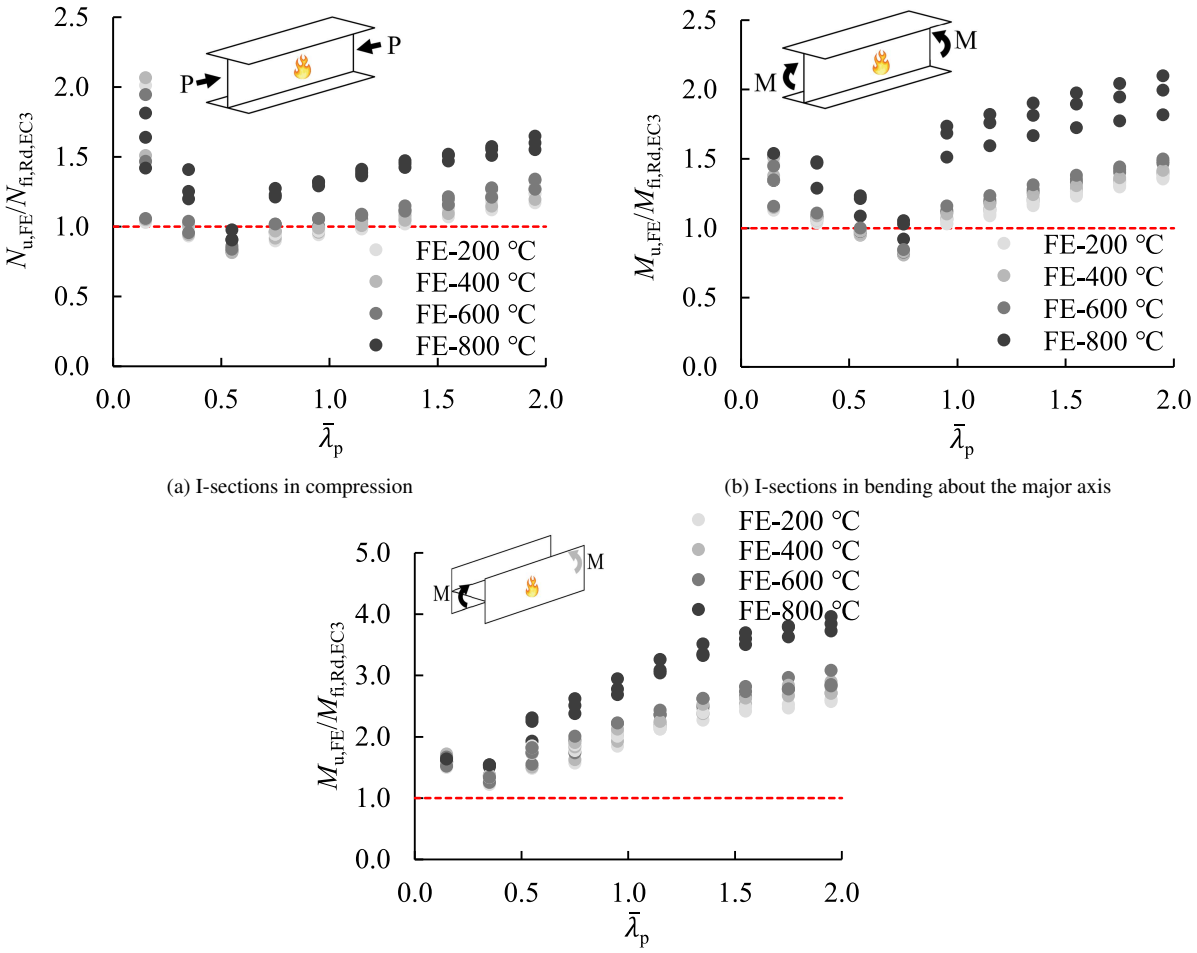

(a) I-sections in compression

(b) I-sections in bending about the major axis

(c) I-sections in bending about the minor axis

Figure 9: Assessment of EN 1993-1-2 [11] against FE results for duplex stainless steel I-sections

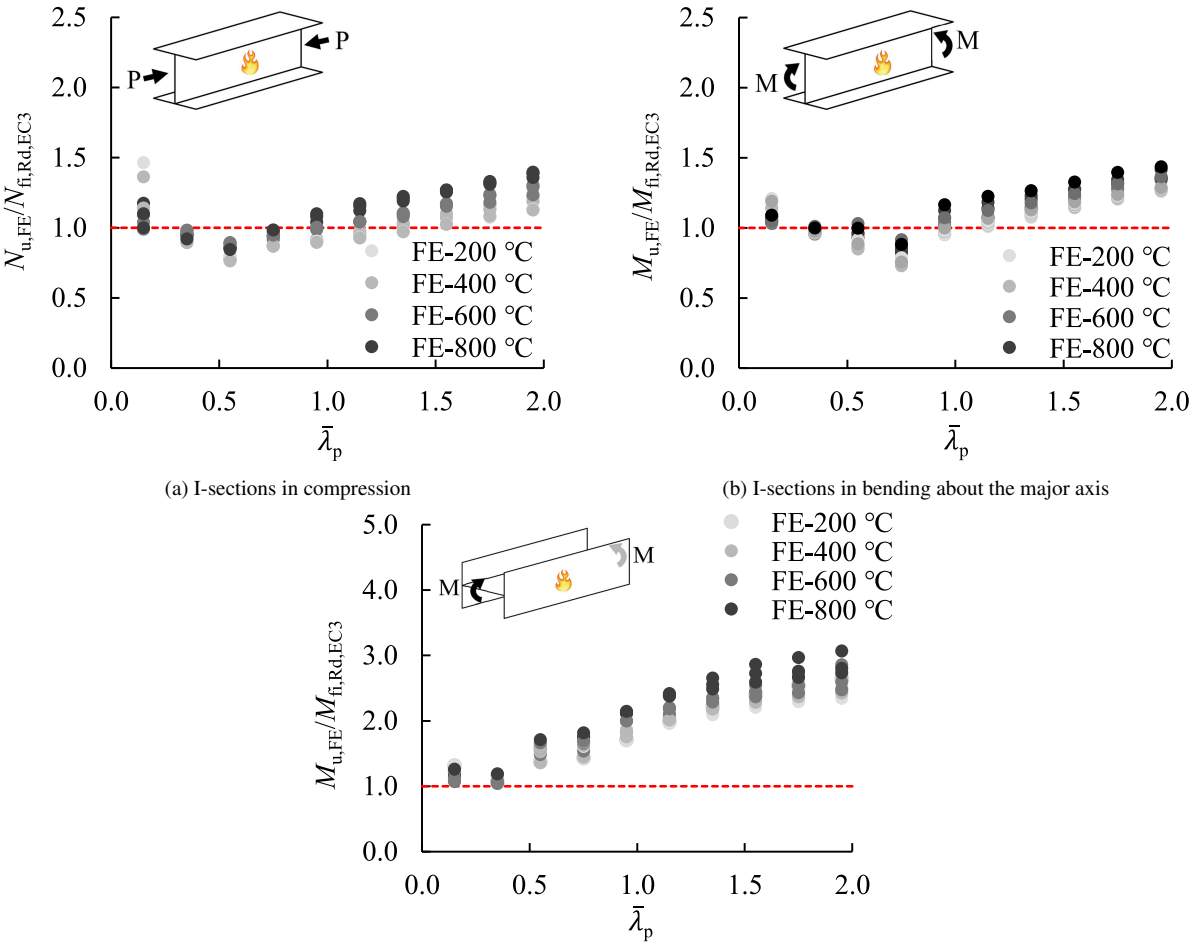

(a) I-sections in compression

(b) I-sections in bending about the major axis

(c) I-sections in bending about the minor axis

Figure 10: Assessment of EN 1993-1-2 [11] against FE results for ferritic stainless steel I-sections

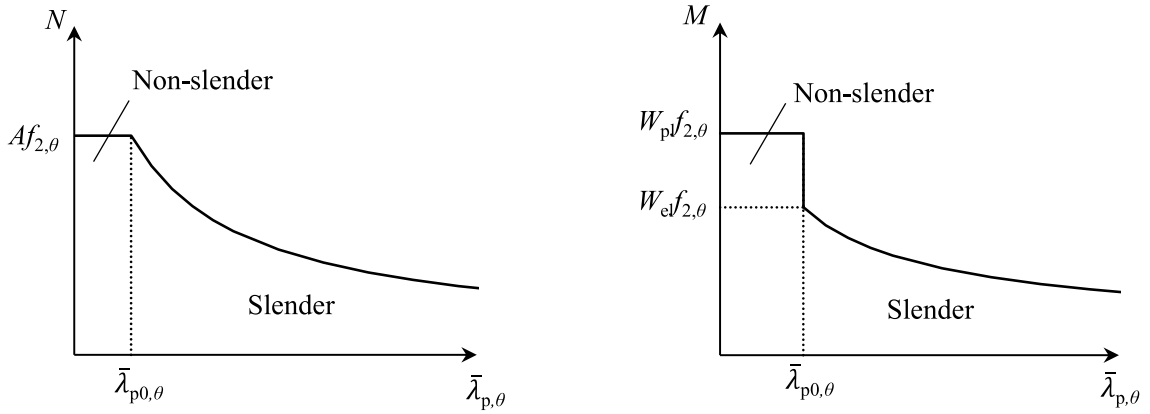

(a) Stainless steel I-sections in compression

(b) Stainless steel I-sections in bending

Figure 11: Illustration of cross-section resistances in design method of [1]

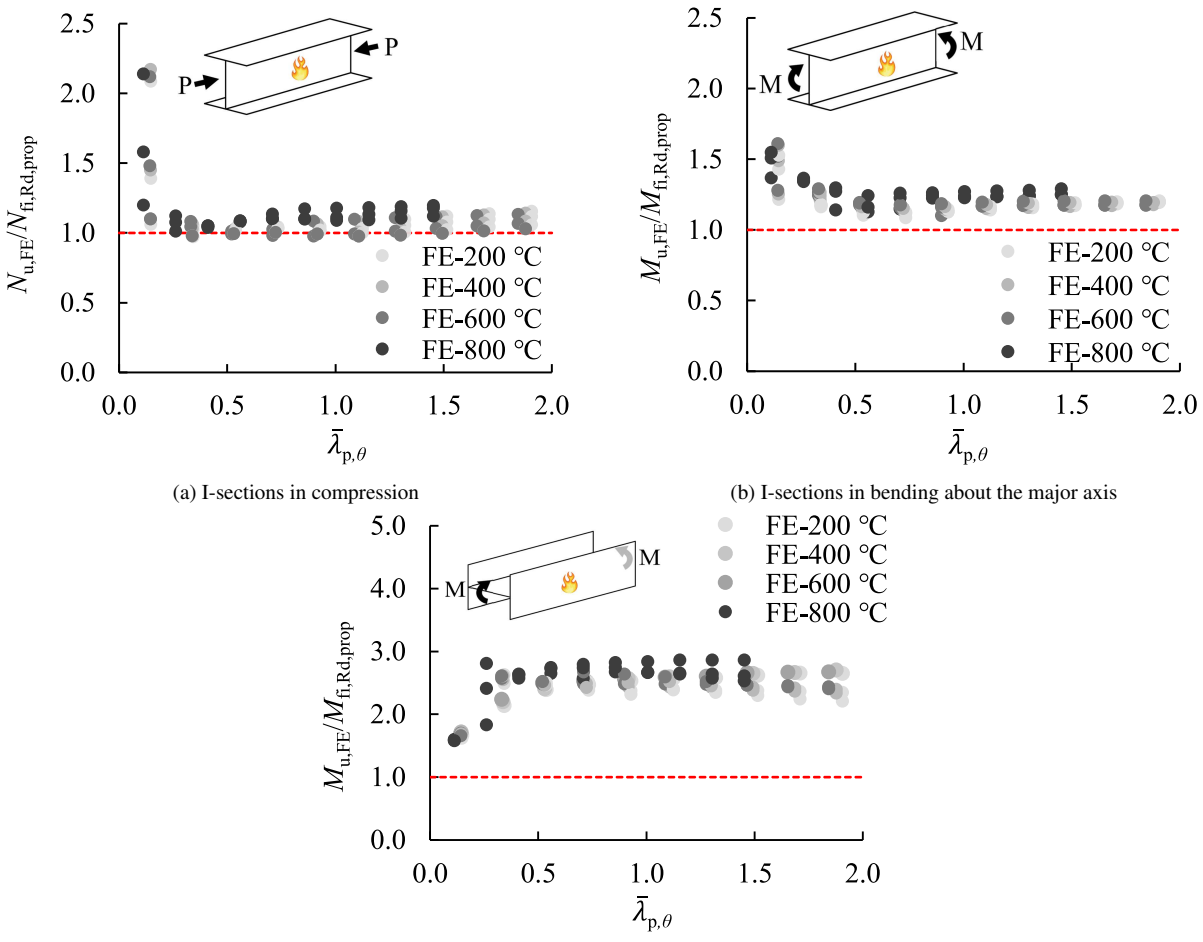

(a) I-sections in compression

(b) I-sections in bending about the major axis

(c) I-sections in bending about the minor axis

Figure 12: Assessment of design method of [1] against FE results for austenitic stainless steel I-sections

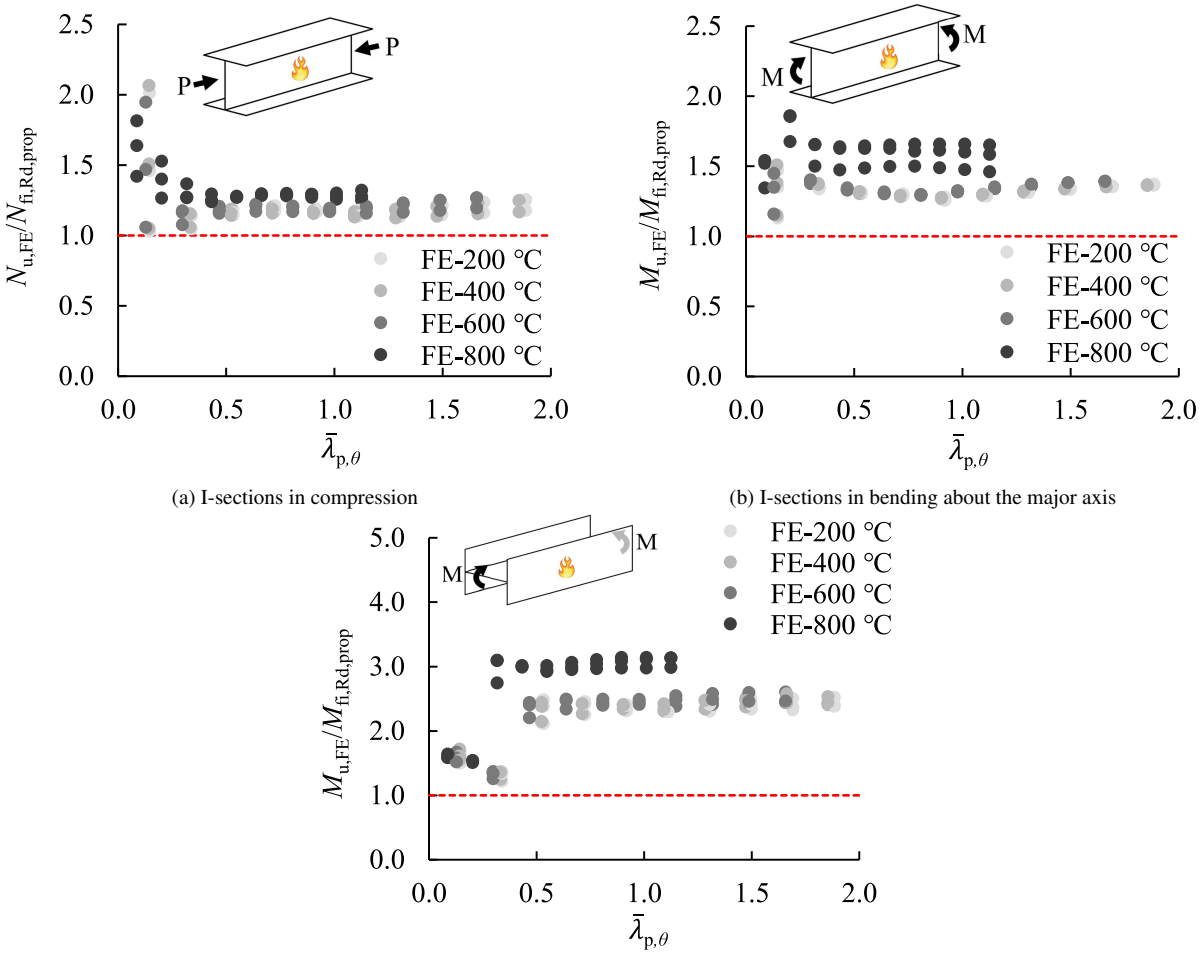

(a) I-sections in compression

(b) I-sections in bending about the major axis

(c) I-sections in bending about the minor axis

Figure 13: Assessment of design method of [1] against FE results for duplex stainless steel I-sections

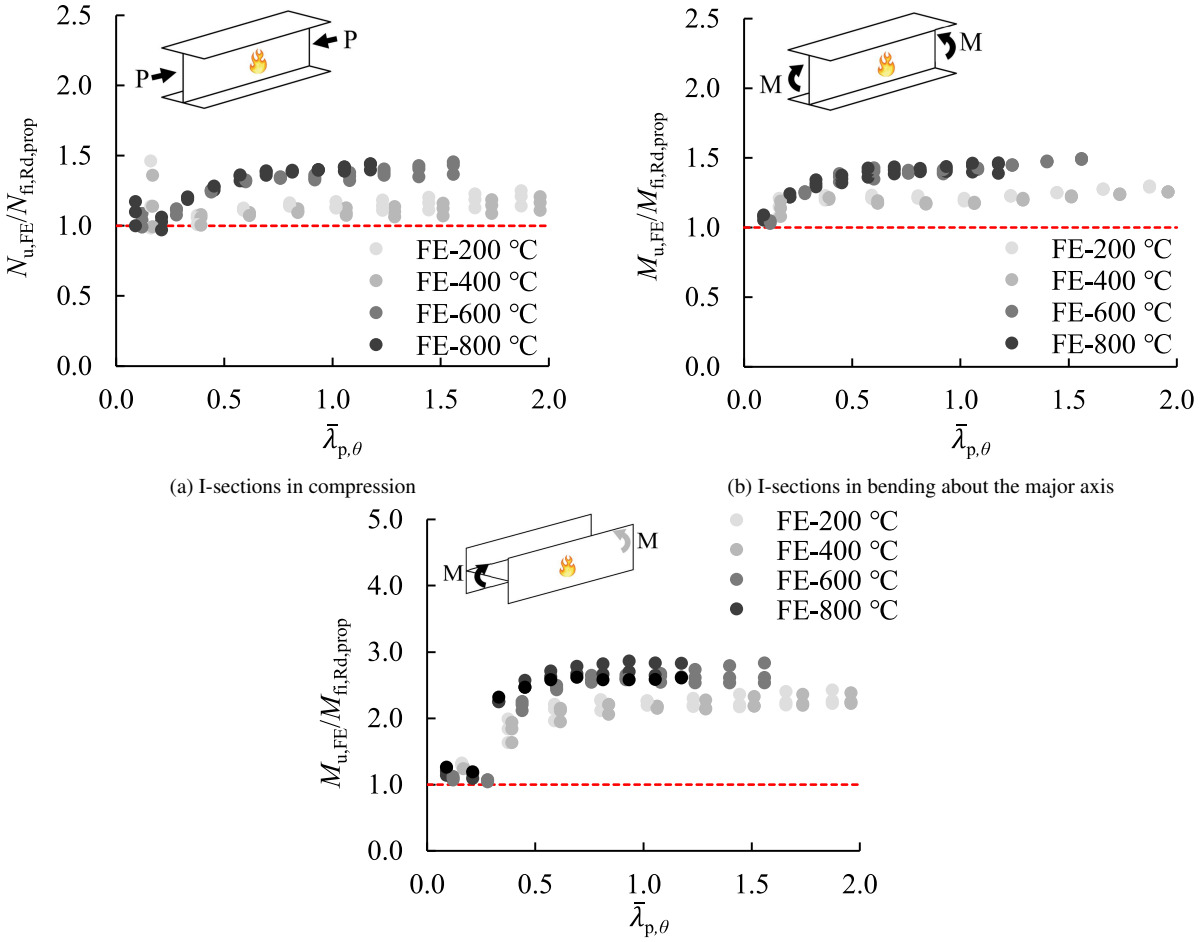

(a) I-sections in compression

(b) I-sections in bending about the major axis

(c) I-sections in bending about the minor axis

Figure 14: Assessment of design method of [1] against FE results for ferritic stainless steel I-sections

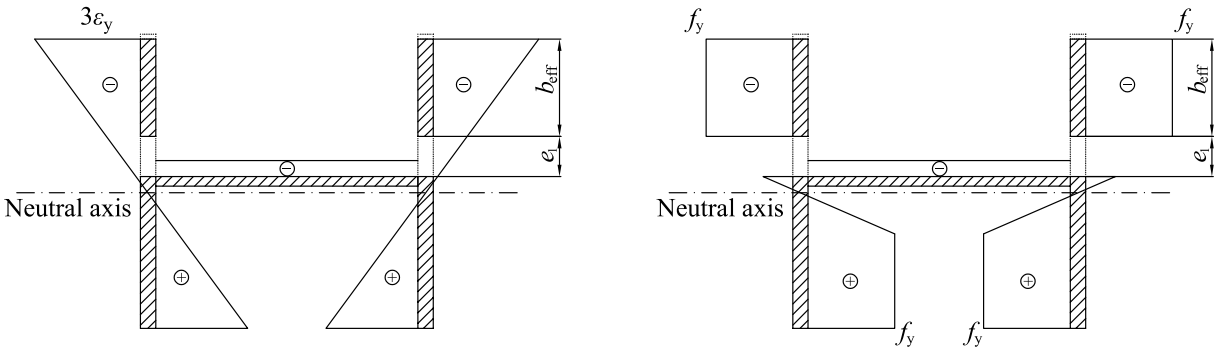

(a) Strain distribution

(b) Stress distribution

Figure 15: Strain and stress distributions in I-sections under minor axis bending based on plastic effective width method proposed by Bambach and Rasmussen [2], with tensile stresses indicated as positive

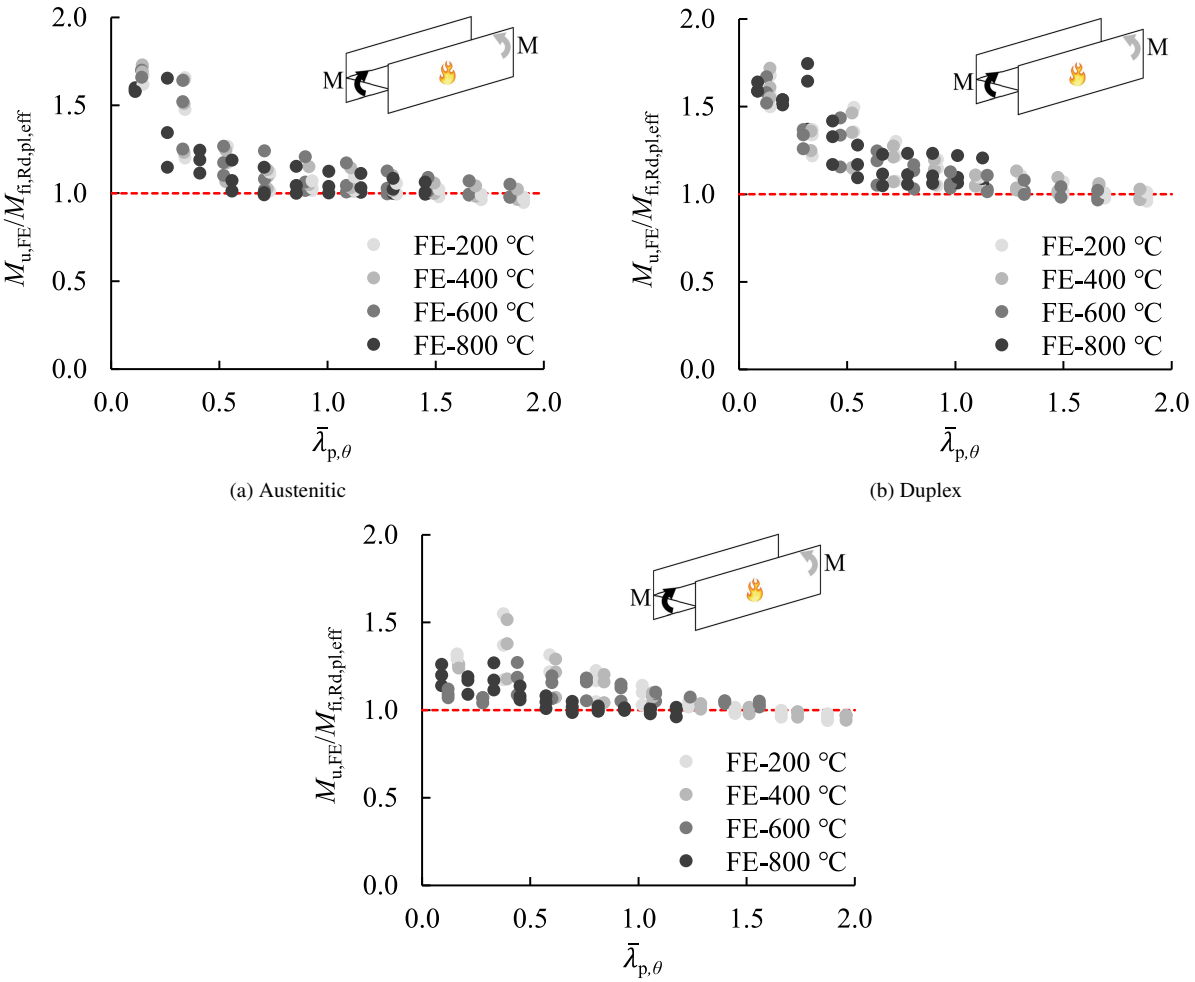

(a) Austenitic

(b) Duplex

(c) Ferritic

Figure 16: Assessment of plastic effective width method of [2] with plate slenderness $\bar{\lambda}_{p,\theta}$ definition of [1] against FE results for stainless steel I-sections under minor axis bending

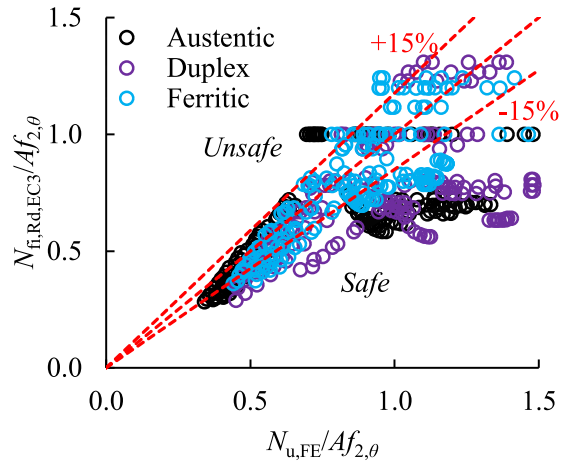

(a) Assessment of EN 1993-1-2 [11] for I-sections in compression

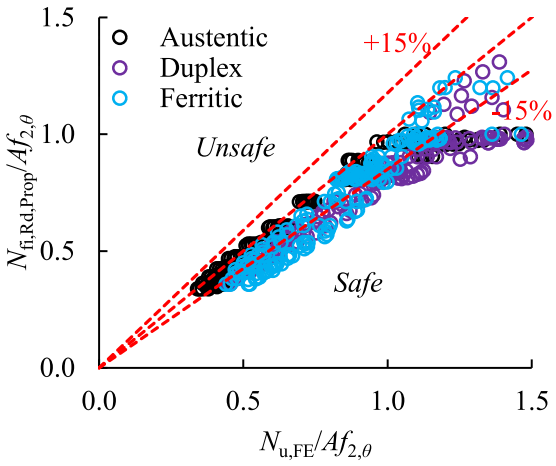

(b) Assessment of design methods of [1] for I-sections in compression

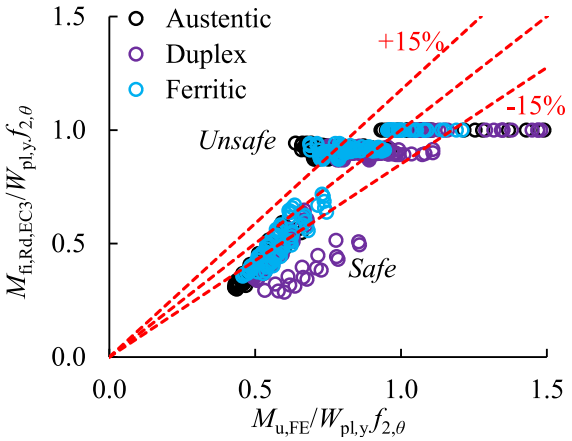

(c) Assessment of EN 1993-1-2 [11] for I-sections in bending about the major axis

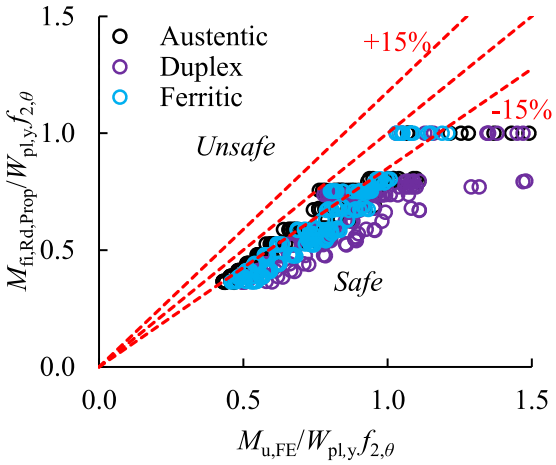

(d) Assessment of design methods of [1] for I-sections in bending about the major axis

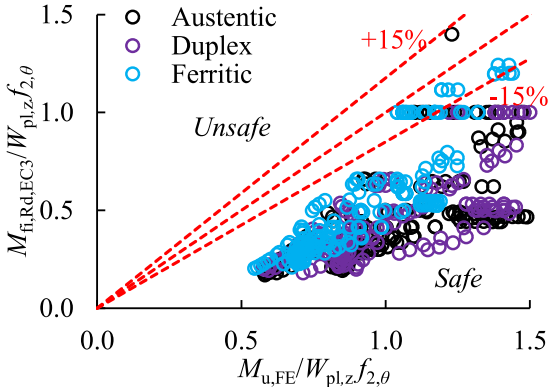

(e) Assessment of EN 1993-1-2 [11] for I-sections in bending about the minor axis

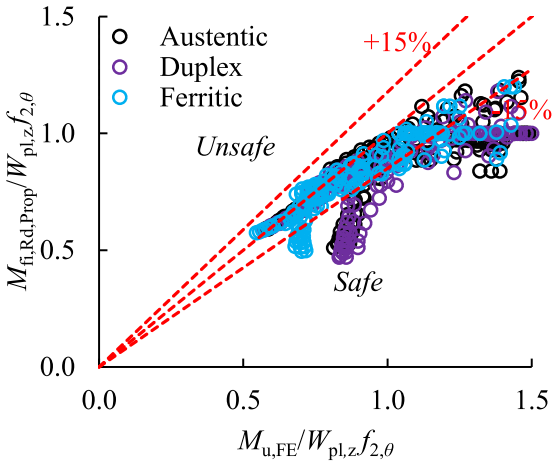

(f) Assessment of design methods of Xing et al. [1] and Bambach and Rasmussen [2] for I-sections in bending about the minor axis

Figure 17: Assessment of EN 1993-1-2 [11] and design methods of Xing et al. [1] and Bambach and Rasmussen [2] against FE results for all stainless steel I-sections

8. Tables

Table 1: Comparison between the load-carrying capacities obtained from stainless steel RHS stub column tests in fire in [36] and those determined through finite element modelling

Section	θ_{cr} (°C)	$N_{u,test}$ (kN)	$N_{u,FE}$ (kN)	$N_{u,FE}/N_{u,test}$
RHS 200×200×5	609	694	653	0.94
RHS 200×200×5	685	567	549	0.97
RHS 200×200×5	764	463	425	0.92
RHS 150×150×3	676	203	216	1.06
RHS 150×150×3	720	165	185	1.12
RHS 150×150×3	588	248	244	0.98

Table 2: Comparison between the load-carrying capacities obtained from beam tests on stainless steel I-sections in fire in [14, 38] and those determined through finite element modelling

Reported by	Section	θ_{cr} (°C)	$M_{u,test}$ (kNm)	$M_{u,FE}$ (kNm)	$M_{u,FE}/M_{u,test}$
Gardner and Baddoo [14]	I 200×150×6	944	17.2	17.4	1.01
	I 120×64	650	15.2	14.4	0.95
Xing et al. [38]	I 248×249×8×13	300	87.25	85.85	0.98
	I 248×249×8×13	400	84.77	84.52	1.00
	I 248×249×8×13	500	82.43	81.82	0.99
	I 248×249×8×13	600	69.56	73.58	1.06

Table 3: Summary of room temperature material properties for austenitic, duplex and ferritic stainless steel grades used in this study

Material grade	E (GPa)	f_y (MPa)	f_u (MPa)	ε_u	n_θ (= n)
Austenitic	200	280	580	0.50	9.1
Duplex	200	530	770	0.30	9.3
Ferritic	200	320	480	0.16	17.2

Table 4: Local plate slenderness values considered in parametric studies

Loading condition	Web slenderness $\overline{\lambda}_{p,w}$	Flange slenderness $\overline{\lambda}_{p,f}$
Compression	0.15, 0.35, 0.55, 0.75, 0.95, 1.15, 1.35, 1.55, 1.75, 2.00	$\overline{\lambda}_{p,f} = \overline{\lambda}_{p,w}$
	0.25	0.35, 0.55, 0.75, 0.95, 1.15, 1.35, 1.55, 1.75, 2.00
	0.35, 0.55, 0.75, 0.95, 1.15, 1.35, 1.55, 1.75, 2.00	0.25
Major axis bending	0.15, 0.35, 0.55, 0.75, 0.95, 1.15, 1.35, 1.55, 1.75, 2.00	$\overline{\lambda}_{p,f} = \overline{\lambda}_{p,w}$
	0.25	0.35, 0.55, 0.75, 0.95, 1.15, 1.35, 1.55, 1.75, 2.00
	0.55, 0.75, 0.95, 1.15, 1.35, 1.55, 1.75, 2.00	0.40
Minor axis bending	0.15, 0.35, 0.55, 0.75, 0.95, 1.15, 1.35, 1.55, 1.75, 2.00	$\overline{\lambda}_{p,f} = \overline{\lambda}_{p,w}$
	0.25	0.35, 0.55, 0.75, 0.95, 1.15, 1.35, 1.55, 1.75, 2.00
	0.35, 0.55, 0.75, 0.95, 1.15, 1.35, 1.55, 1.75, 2.00	0.25

Table 6: Width-to-thickness limits for plate classification at room temperature in EN 1993-1-4 [6]

Element	Class 1	Class 2	Class 3
Internal element subjected to compression	33ε	35ε	37ε
Internal element subjected to bending	72ε	76ε	90ε
Outstand flange subjected to compression	9ε	10ε	14ε

Table 8: Definition of cross-section resistances in design method of [1]

Cross-section classification	Design resistance in compression	Design resistance in bending
Non-slender	$N_{fi,t,Rd} = A f_{2,\theta}/\gamma_{M,fi}$	$M_{fi,t,Rd} = W_{pl} f_{2,\theta}/\gamma_{M,fi}$
Slender	$N_{fi,t,Rd} = A_{eff} f_{2,\theta}/\gamma_{M,fi}$	$M_{fi,t,Rd} = W_{eff} f_{2,\theta}/\gamma_{M,fi}$

Table 5: Flange and web thicknesses of I-sections with $\overline{\lambda}_{p,w}$ equal to $\overline{\lambda}_{p,f}$ in parametric studies

Grade	Loading conditions	Slenderness / Thickness	0.15	0.35	0.55	0.75	0.95	1.15	1.35	1.55	1.75	1.95
Austenitic	Compression	t_f (mm)	18.36	8.18	5.29	3.91	3.10	2.57	2.19	1.91	1.70	1.52
		t_w (mm)	8.31	4.71	3.20	2.42	1.94	1.62	1.39	1.22	1.09	0.98
	Major axis bending	t_f (mm)	19.36	8.42	5.39	3.96	3.14	2.59	2.21	1.93	1.71	1.53
		t_w (mm)	3.29	1.91	1.31	0.99	0.79	0.66	0.57	0.50	0.44	0.40
	Minor axis bending	t_f (mm)	15.83	7.09	4.59	3.39	2.69	2.23	1.90	1.66	1.47	1.32
		t_w (mm)	8.97	4.83	3.25	2.45	1.96	1.64	1.40	1.23	1.09	0.98
Duplex	Compression	t_f (mm)	25.06	11.09	7.20	5.33	4.24	3.51	3.00	2.62	2.33	2.09
		t_w (mm)	9.01	6.02	4.22	3.23	2.61	2.19	1.89	1.66	1.48	1.33
	Major axis bending	t_f (mm)	26.59	11.52	7.38	5.44	4.30	3.56	3.04	2.65	2.35	2.11
		t_w (mm)	3.46	2.44	1.72	1.32	1.07	0.90	0.77	0.68	0.60	0.54
	Minor axis bending	t_f (mm)	21.46	9.61	6.24	4.63	3.68	3.05	2.61	2.28	2.02	1.82
		t_w (mm)	10.31	6.25	4.31	3.28	2.64	2.21	1.90	1.67	1.49	1.34
Ferritic	Compression	t_f (mm)	19.57	8.72	5.64	4.17	3.31	2.74	2.34	2.04	1.81	1.63
		t_w (mm)	8.54	4.97	3.40	2.57	2.07	1.73	1.49	1.30	1.16	1.04
	Major axis bending	t_f (mm)	20.68	8.99	5.76	4.24	3.35	2.77	2.36	2.06	1.83	1.64
		t_w (mm)	3.37	2.02	1.39	1.05	0.85	0.71	0.61	0.53	0.47	0.43
	Minor axis bending	t_f (mm)	16.86	7.56	4.89	3.62	2.87	2.38	2.03	1.78	1.57	1.41
		t_w (mm)	9.30	5.11	3.45	2.60	2.09	1.74	1.50	1.31	1.17	1.05

Table 7: Definition of cross-section resistances in **EN 1993-1-2** [11]

Cross-section classification	Design resistance in compression	Design resistance in bending
Class 1 and 2	$N_{\mathrm{fi,t,Rd}} = A f_{2,\theta}/\gamma_{\mathrm{M,fi}}$	$M_{\mathrm{fi,t,Rd}} = W_{\mathrm{pl}} f_{2,\theta}/\gamma_{\mathrm{M,fi}}$
Class 3	$N_{\mathrm{fi,t,Rd}} = A f_{2,\theta}/\gamma_{\mathrm{M,fi}}$	$M_{\mathrm{fi,t,Rd}} = W_{\mathrm{el}} f_{2,\theta}/\gamma_{\mathrm{M,fi}}$
Class 4	$N_{\mathrm{fi,t,Rd}} = A_{\mathrm{eff}} f_{\mathrm{p0.2},\theta}/\gamma_{\mathrm{M,fi}}$	$M_{\mathrm{fi,t,Rd}} = W_{\mathrm{eff}} f_{\mathrm{p0.2},\theta}/\gamma_{\mathrm{M,fi}}$

Table 9: Accuracy assessment of EN 1993-1-2 [11] and design methods of Xing et al. [1] and Bambach and Rasmussen [2] against numerical results for all stainless steel I-sections

Loading condition	Grade	EN 1993-1-2		Design methods of [1, 2]	
		$\varepsilon_{\mathrm{mean}}$	$\varepsilon_{\mathrm{COV}}$	$\varepsilon_{\mathrm{mean}}$	$\varepsilon_{\mathrm{COV}}$
Compression	Austenitic	1.24	0.265	1.13	0.158
	Duplex	1.33	0.263	1.26	0.117
	Ferritic	1.12	0.159	1.18	0.102
Major axis bending	Austenitic	1.07	0.212	1.23	0.082
	Duplex	1.17	0.239	1.38	0.107
	Ferritic	1.03	0.151	1.28	0.087
Minor axis bending	Austenitic	2.41	0.328	1.26	0.184
	Duplex	2.39	0.315	1.30	0.174
	Ferritic	1.93	0.286	1.12	0.101

Table 10: Reliability assessment of EN 1993-1-2 [11] and design methods of Xing et al. [1] and Bambach and Rasmussen [2] against numerical results for all stainless steel I-sections. Values are given as percentages

Loading condition	Grade	EN 1993-1-2			Design methods of [1, 2]		
		Crit. 1	Crit. 2	Crit. 3	Crit. 1	Crit. 2	Crit. 3
Compression	Austenitic	7.81*	28.65*	-13.89	0.00	10.94	-10.06
	Duplex	4.69*	17.71	-19.86	0.00	0.00	-19.58
	Ferritic	6.28*	32.98*	-8.27	0.00	2.60	-14.51
Major axis bending	Austenitic	25.95*	48.65*	-2.04	0.00	0.00	-17.92
	Duplex	5.35*	29.95*	-10.66	0.00	0.00	-26.67
	Ferritic	13.30*	48.94*	-0.84	0.00	0.00	-21.36
Minor axis bending	Austenitic	0.00	0.50	-53.04	0.00	11.00	-18.17
	Duplex	0.00	0.00	-53.66	0.00	6.00	-20.99
	Ferritic	0.00	0.00	-42.94	0.00	13.50	-9.76

*Reliability criterion of [44] not satisfied.